DEVELOPMENT OF AN OPTICAL SPECTROSCOPIC METHOD TO DETECT NEUROHEMODYNAMIC CHANGES INDUCED BY PAIN IN RATS

by

SWETA NARVENKAR

Presented to the Faculty of the Graduate School of

The University of Texas at Arlington in Partial Fulfillment

of the Requirements

for the Degree of

MASTER OF SCIENCE IN BIOMEDICAL ENGINEERING

THE UNIVERSITY OF TEXAS AT ARLINGTON

December 2009

ACKNOWLEDGEMENTS

Research is always a group effort and I would like to take this valued occasion to thank all my colleagues, collaborators & professors who laid the foundation for my research and overall experience during my Masters.

A heartfelt and sincere thank you to my mentor, Dr. Hanli Liu, who entrusted confidence in my naïve capabilities and gave me an opportunity to develop my research skills under her guidance.

My inestimable gratefulness to my Parents, my Brother, my fiancée and God for their constant encouragement, their trust in my potentials and their love and blessings always rendered to me.

I would also like to thank Dr. Yaun Bo Peng for giving me the invaluable knowledge, Mr. Ji Wei He for experimental set up, rat surgery and for assisting me in acquiring the data and also for their important inputs. My thanks also go out to Dr. George Alexandrakis for teaching me the valued fundamentals of optics during his coursework and also for accepting my request to be a committee member.

Lastly, very special thanks to Nancy Rowe for her guidance in statistics for my project, Vikrant Sharma, Nimit Patel and Yajuvendra Rathore for their research support and encouragement during my thesis.

November 18, 2009

ABSTRACT

DEVELOPMENT OF AN OPTICAL SPECTROSCOPIC METHOD

TO DETECT NEUROHEMODYNAMIC CHANGES

INDUCED BY PAIN IN RATS

Sweta Narvenkar, M.S.

The University of Texas at Arlington, 2009

Supervising Professor: Hanli Liu

In my optical spectroscopy study, multi-channel, thin optical probes with short source-detector separation have been implemented, calibrated, and used along with a multi-channel spectrometer as a quantitative technique to observe changes in vascular hemoglobin concentration and hemoglobin oxygen saturation as well as light scattering of tissues. Each of the four needle probes used in my study consists of two bifurcated fibers; one fiber is connected to a halogen light source and the other fiber to a CCD-array spectrometer having a spectral window from 450 nm to 900 nm. Each fiber is 100 micron in diameter. As we utilized the four probes individually and simultaneously, a source multiplexer and a multi-channel spectrometer were used during the measurement. For quantification of tissue physiological parameters, each probe needed to be calibrated to remove the instrumentation effects.

The laboratory experiments using liquid tissue phantoms were conducted to calibrate the probes and to validate the algorithm that was developed to quantify oxygenated [HbO] and deoxygenated [Hb] hemoglobin concentrations and scattering coefficients. These calibrated probes were then applied for the pain study in rats. Two probes were placed on the spinal cord and two on the primary somatosensory (S1) region of the rat brain, each on the ipsilateral and contralateral sides of the rat. While the paw of the rat was stimulated using electrical stimulations, hemodynamic responses were acquired at the four locations on the rat. The results showed a significant increase in [HbO] and a decrease in [Hb] at the ipsilateral side of the spinal cord and contrlateral side of the S1 region of the brain, caused by the electrical stimulation at the paw. My study demonstrates that multi-channel reflectance spectroscopy is a useful tool to study pain mechanism at different central nervous sites using animal models.

TABLE OF CONTENTS

ACKNOWLEDGEMENTS ii

ABSTRACT iii

LIST OF ILLUSTRATIONS viii

LIST OF TABLES x

Chapter Page

1. INTRODUCTION 1

1.1 NIRS Background 1

1.2 Pain Study Background 3

1.2.1 Perception of Pain 3

1.2.2 Classification of Pain 3

1.2.3 Nociceptors 4

1.2.4 Conduction of nociception 6

2. INSTRUMENTATION 8

2.1 Introduction 8

2.2 Instrumentation 9

2.2.1 Light Source 10

2.2.2 Optical multiplexer 10

2.2.3 Spectrometer 11

2.2.4 Optical Fiber 13

2.2.5 Data Acquisition 14

3. REFLECTANCE MODEL 15

3.1 Reflectance model for short source-detector separation 16

3.2 Forward calculation 17

3.2.1 Calculation of absorption and reduced scattering coefficients 18

3.2.2 Determination of k_1 and k_2 20

3.3 Inverse Calculation 20

3.4 Phantom Studies 21

3.4.1 Experimental Set up 21

3.5 Modified Beer Lambert's Law 25

3.6 Look-Ahead Distance 28

4. PAIN STUDY 32

4.1 Introduction 32

4.2 Animal Preparation and Experimental Protocol 32

4.2.1 Baseline Measurements 34

4.2.2 Stimulations 35

4.3 Data Analysis 35

4.4 Result and Discussion 38

4.4.1 Spinal Cord 38

4.4.2 Brain 41

4.4.3 Comparisons between spinal cord and brain 43

5. CONCLUSION AND FUTURE WORK 49

APPENDIX

A. PHOSPHATE BUFFERED SALINE 51

REFERENCES 53

BIOGRAPHICAL INFORMATION 57

LIST OF ILLUSTRATIONS

Figure Page

1.1 The optical pathway in tissues 1

1.2 The pathway of different pain stimulation to the spinal cord..... 5

1.3 The conduction of pain from the periphery to the CNS 6

2.1 The absorption spectra of oxygenated and deoxygenated hemoglobin and water 8

2.2 The Light Source..... 10

2.3 The Multiplexer..... 11

2.4 The principle of operation of the spectrometer 12

3.1 Schematic diagram of phantom, illustrating positions of the thin fiber probe and ISS Oximeter probe. The thin probe tip was facing vertically down, 2-3 cm below the solution surface, and 4-5 cm away from the walls of the container. The probe position of ISS Oximeter is also shown 22

3.2 The scatter plot for (Rp/μ_s') versus μ_a' (λ), k_1 and k_2 are the intercept and the slope, respectively 24

3.3 The change in [HbO] and [Hb] during yeast measurements and pumping of oxygen..... 27

3.4 The effect of increasing intralipid concentration on the change in the [HbO] and [Hb] keeping blood concentration constant 28

3.5 The schematic diagram of the experimental set up to determine the LAD of the probes of 700um and 100um source-detector separation. The above set up is immersed in a intralipid phantom 30

3.6 The experimental results of normalized slope versus the distance between the probes and the black capillary..... 31

4.1 The experimental set up and the probe placement on the brain and spinal cord 34

4.2 The use of one way ANOVA in analyzing block design 38

4.3 An increase in [HbO] at the ipsilateral side of the spinal cord due to electrical stimulation of 10V, 10Hz, 1ms pulse width 39

4.4 A decrease in [Hb] at the ipsilateral side of the spinal cord due to electrical stimulation of 10V, 10Hz, 1ms pulse width 40

4.5 An increase in [HbO] at the contralateral side of the brain in the S1 region, from the baseline due to electrical stimulation of 10V, 10Hz, 1ms pulse width 42

4.6 A decrease in [Hb] at the contralateral side of the brain in the S1 region, from the baseline due to electrical stimulation of 10V, 10Hz, 1ms pulse width 42

4.7 The normalized change in [HbO], at the spinal cord and brain, due to 10V electrical stimulation at the paw 44

4.8 The time response to peak, [HbO] changes, at the spinal cord and the S1 region in the brain due to 10V electrical stimulation 45

4.9 The time spread of the [HbO] changes, at the spinal cord and the S1 region in the brain due to 10V electrical stimulation 46

4.10 The relative [HbO] changes for each of the five blocks, for Rat 7, at the ipsilateral side of the spinal cord, due to electrical stimulation of 10V at the hind paw 47

4.11 The relative average [HbO] changes, for Rat 7, at the ipsilateral side of the spinal cord, due to electrical stimulation of 10V at the hind paw. 47

LIST OF TABLES

Table Page

3.1 The different Blood and intralipid concentrations used in the phantom study, as well as the k_1 and k_2 for each condition 23

4.1 The k_1 *and* k_2 values used in the pain study 37

4.2 The statistical results for the ipsilateral side of the spinal cord in response to electrical stimulation on the paw 41

4.3 The statistical results for the contralateral side of the brain in response to electrical stimulation on the paw 43

4.4 The maximum amplitude of change in [HbO] at the spinal cord and the brain, in response to 10V electrical stimulation at the paw. The p-value < 0.05, shows that they are statistically different..... 43

CHAPTER 1

INTRODUCTION

1.1 NIRS Background

Hemoglobin oxygenations of muscles [1-3], brain [4, 5] and animal tumors [6,7] have been investigated by the use of optical spectroscopy with visible and near infrared light. When light passes through the tissues, it can be absorbed or scattered and then reflected back to the detector. The light that is reflected carries a lot of information about the underlying tissue. The broader the source-detector separation, the deeper the light penetrates. By separating the effects of absorption and scattering of light in tissues, it is possible to calculate concentration of the chromophores and scattering coefficients. The propagation of light in tissue is complex: the photons do not travel along a straight path in tissue as they do in a clear medium; instead, they bounce off or are scattered due to many boundaries of tissue substructures. This phenomenon of light scattering causes random propagation of photons in tissue. Photons passing through tissues usually form a "banana" pattern (Fig. 1), the optical pathway in the tissues; hence the measurement is most sensitive to objects found in that volume.

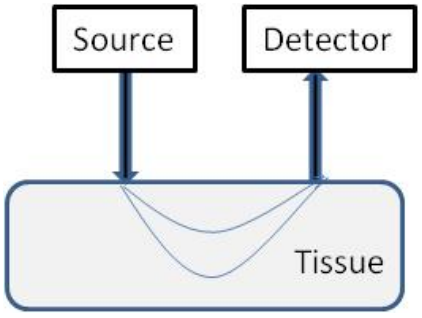

Figure 1.1 The optical pathway in tissues

Coefficient of absorption can be described as the probability of a photon for being absorbed in the tissue, over a given distance. The absorption coefficient, μa, is the average number of absorption events per distance and is usually given in unit of 1/cm = cm^{-1}. Tissues contain chromophores such as oxy-hemoglobin and deoxy-hemoglobin, which possess μa values that depend on the chromophore's concentration [32].

Light scattering is the process of elastic scattering of a photon traveling in a medium. In this process the photon is not destroyed by absorption; only its direction of propagation is changed in each step. The scattering coefficient, μs, is the average number of scattering events per light travel distance in a medium. It is usually given in unit of 1/cm. As scattering events redirect the photon paths randomly, the process causes blur and reduces contrast [32].

Near Infrared Spectroscopy (NIRS) is one of the simplest techniques used to study physiological, homodynamic changes and properties of biological tissues. Light that is incident on tissues undergoes multiple scattering and absorption. Optical imaging can be done either in the transmission or reflectance mode. A few millimeters or centimeters away from the source, a detector can detect light that are scattered in the tissue, which could give useful information about the underlying tissue. Attenuation of light in the visible region (450-650 nm) is strong in tissues, as compared to the attenuation in the near infrared (700-900 nm) region. This attenuation is due to oxygenated hemoglobin (HbO) and deoxygenated hemoglobin (Hb), tissue chromophores, concentration of which can be calculated by studying their variations in the visible wavelength region [33].

A regular optical spectroscopic system is a relatively inexpensive, simple in design and construction and is readily suited for the determination of μ_a and μ_s' over large, continuous ranges of wavelengths compared to other techniques. The reflectance system used in this study is a real time monitoring system that is built with a broadband white light source and a

broadband data acquisition spectrometer that is accomplished with the use of a CCD array. Using this system, the acquisition time is significantly reduced and permits rapid data acquisition [33].

Optical needle probes with very small source-detector separations have also been used previously by our group and other groups to differentiate between deep brain structures [10] and monitor oxygenation levels in animal tumors [7, 11]. Previously performed studies have been restricted to the determination of relative concentrations of tissue chromophores, oxy-hemoglobin and deoxy-hemoglobin, or require reflectance or transmittance measured at multiple source detector separations for calculation of absolute chromophore concentrations. Development of a short-separation fiber optic system to quantify oxy-hemoglobin and deoxy-hemoglobin concentrations with a single source detector separation would result in significant simplification of instrumentation hardware.

1.2 Pain Study Background

1.2.1 Perception of Pain

Pain is an unpleasant sensory and emotional experience associated with actual or potential tissue damage [34]. Even though pain is mediated by nervous system, distinction between pain and the neural mechanisms of nociception – the response to actual or perceived tissue damage- is critical both experimentally and clinically. Certain tissues are equipped with specialized receptors, known as nociceptors, which are activated by noxious insults to peripheral tissues. Nociception will not necessarily lead to the experience of pain [34].

1.2.2 Classification of Pain

Pain can be classified as temporal or physiological. When pain is classified by time, it can be acute or chronic. A second classification of pain is physiological, which includes nociceptive pain, which can be divided into somatic and visceral types of pain [33-35].

Acute pain has a short duration, whereas chronic pain may be present after treatment is completed. Acute pain has an identifiable pathology, whereas chronic pain has a possibly unclear pathology [33-35]. Chronic pain often occurs in the absence of ongoing illness or after healing is completed. A fundamental difference between the acute and chronic pain is that acute pain is persistent only during illness and disappears once the illness is cured, but chronic pain is persistent even after the illness is cured.

Pain can also be classified into two broad classes, nociceptive and neuropathic. Nociceptive pain results from direct activation of nociceptors in the skin or soft tissue in response to tissue injuries and usually arises from accompanying inflammation. Neuropathic pain is a result of direct injury to nerves in the peripheral or central nervous system.

1.2.3 Nociceptors

The neurons called as nociceptors respond only to extreme pressure or temperature. This means they sense only painful stimuli.

These nociceptive neurons have a high threshold and are comparatively slower in conduction as to the other peripheral axons. Peripheral nerve axons are divided into the following, A, B and C fibers, according to their conduction velocity. The myelinated fibers are A and B fibers, while the C fibers is not myelinated. Aα, Aβ, Aγ, and Aδ classes are the subdivisions of A fibers in descending order of their conduction velocity. Aβ fibers carry ordinary sensory, while pain sensation is carried by Aδ and C fibers [33-35]. The Aδ fibers conduct signals relatively slow, at the speed of 5-30 m/s in mammals, whereas C fibers conduct at only 0.5-2 m/s. At this rate, pain from an injury to the lower limb would take one to three seconds to reach the brain [33-35]. The Aδ fibers conduct pain caused by extreme pressure and temperature such as the one from activation of mechonosensitive nociceptors as well as the thermo sensitive nociceptors. This pain is perceived as sharp and localized. The C fibers in

contrast cause a diffuse, burning sensation that tends to be persistent. C fibers can be activated by numerous stimuli including pressure, temperature and chemicals released by damaged cells in their vicinity [33-35]. When there is an injury, there is an activation of the nociceptors in the damaged region. Pain is perceived as a result of the Aδ fibers. Even after the stimulation is withdrawn, there is a continuous pain sensation. This is carried by the C fiber (see Fig. 1.2). If the injured region is again exposed to the painful stimulations or even lesser than before stimulation, there exists an increased perceived pain sensation. That phenomenon is called *hyperalgesia*, or enhanced pain sensation in the injured area. Apparently the pain receptors now have lower thresholds as a result of the injury, and thus giving painful responses to stimuli they would ordinarily ignore. Hyperalgesia involves an amplification of the pain signal. This amplification can occur in the periphery or in the spinal cord or in both locations. This may be caused by proinflammatory molecules released at the site of injury. The presumed function of this phenomenon is to prevent re-injury of the region while it is healing.

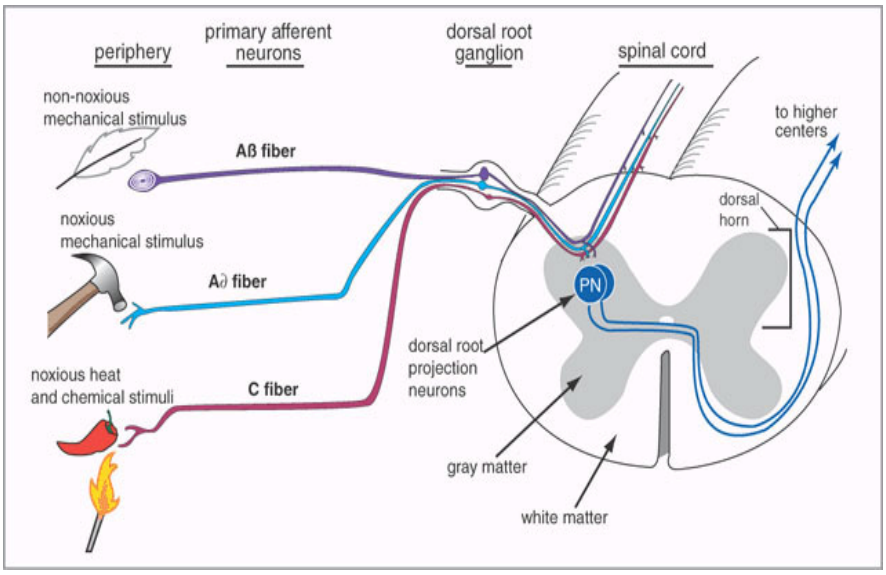

Figure 1.2 The pathway of different pain stimulation to the spinal cord [38]

1.2.4 Conduction of nociception

The organization of the pain conducting pathways is different from that of the ordinary somatosensory pathways. There are some differences between the part of the somatic sensory system that detects ordinary stimuli and the part that detects extreme, and therefore painful, stimuli. The primary pain neurons, the nociceptors, form their first synapses on other neurons in the dorsal horn of the spinal cord. Cell bodies of the pain receptor neurons are located within dorsal root ganglia whose receptive endings are located in the periphery. They are called the dorsal horn of the spinal cord, which make synapses on neurons that project to the thalamus and then to the somatic sensory cortex. After axons synapses at the spinal cord, it goes up the spinal cord on the contralateral side from the original nociceptive neuron. These axons pass through the medulla and project directly to the thalamus where they make synapses on neurons that project in turn to the somatic sensory cortex.

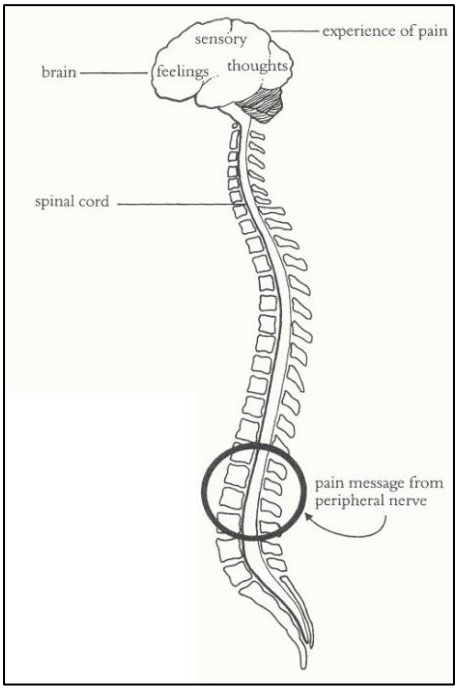

Figure 1.3 The conduction of pain from the periphery to the CNS [39]

As discussed earlier, nociceptive afferent fibers terminate mainly in the dorsal horn of the spinal cord. The dorsal horn can be divided into six classes, based on the cytological features. Distinct functions are conveyed by different classes of primary afferent neurons terminating in the dorsal horn at the spinal cord. Hence, there is a close correlation between functional and anatomical organization of the dorsal horn.

The *Gate Control Theory* explains that pathways that descend from the brain to the dorsal horn of the spinal cord are capable of blocking the transmission of pain information in the spinal cord, and thus preventing the pain sensation from reaching the brain.

Most of these neurons in the marginal layer respond exclusively to noxious stimulation and project to higher brain centers. Nociceptive information is carried from the spinal cord to brain through five major ascending pathways: spinothalamic, spinorecticular, spinomesencephalic, cervicothalamic and spinohypothlamic tracts [19]. Largest nerve in the body, the *sciatic nerve* begins from nerve roots in the lumbar part of the spinal cord and extends through the buttock area to send nerve endings down to the legs. This sciatic nerve carries signals to the spinal cord from the lower periphery. Hence, any stimulation in the lower limbs will carry the pain signal from the sciatic nerve up to the spinal cord.

CHAPTER 2

INSTRUMENTATION

2.1 Introduction

This chapter describes the design and development of a steady-state, broadband, optical spectroscopic system to evaluate the changes in chromophore concentrations, that is, oxygenated and deoxygenated hemoglobin concentration and reduced scattering coefficients.

Optical spectroscopy has been used earlier to monitor hemoglobin concentrations and their changes in biological tissues, which was basically in a relative form. It was also used by our group to characterize cancer and normal tissues based on the difference in the oxygenated and deoxygenated hemoglobin in blood, which may lead to new information that is related to "patho-physiologic processes of tissues such as angiogenesis and hypoxia" [33]. Optical spectroscopic methods utilize a minimum of two wavelengths, one above and one below the wavelength at which oxygenated hemoglobin and deoxygenated hemoglobin have the same molar absorptivity, 750nm and 830nm, as shown in figure 2.1.

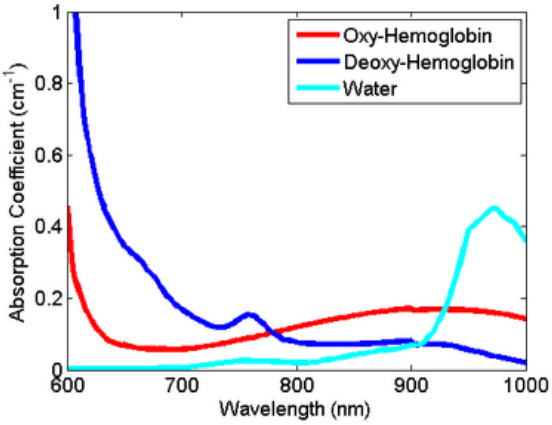

Figure 2.1 The absorption spectra of oxygenated and deoxygenated hemoglobin and water

The design, construction and operation of a steady state, broadband spectroscopic system is described in section 2.2. Each of the four channels of the multiplexer transmits broadband NIR light at 350–1000 nm. The multiplexer has one input from the light source which is then given to different channels of the multiplexer one at a time in an alternating pattern. The spectra from a tissue phantom made up of blood and intralipid or from animal tissue are obtained one at a time from each of the four detector channels of the multichannel spectrometer, which are co-located with the source channels (optical probes). [33]

2.2 Instrumentation

The basic function of this optical system is to measure the complete spectrum over the wavelength range of 450–1000 nm from four fibers detecting the reflected light from the tissue phantom, to which four corresponding fibers delivered light. Four individual, bifurcated optical fiber needle probes have formed the four light delivery fibers and the four detecting fibers. The system uses a time-sharing detection scheme such that each light delivery fiber is illuminated in sequence, one at a time, and reflected light is captured by the respective detecting fiber and sent to one of the channels of an 8-channel spectrometer, one at a time.

The system consists of four major components:

1) One broadband CW light source,

2) Optical multiplexer to multiplex the light from one light source into four channels,

3) 8-channel CCD array spectrometer to detect the light reflected from the surface of the sample, and

4) Four optical fiber bundles with bifurcated fibers for each.

Light is transmitted from the light source to the optical multiplexer, which multiplexes the light source into four light channels. Then, light from each of the four channels are delivered in sequence, one at a time, to the surface of a tissue phantom or the animal tissue, by one of the

light transmitting optical fibers; then, the reflected light is collected by the respective detection fiber and sent to the respective channel of the CCD multichannel spectrometer.

2.2.1 Light source

The broadband optical system uses a fiber-optic light source (Illumination Technologies, Inc. Model 3900 DC regulated, Light Feedback Fiber Optic Light source), as shown in figure 2.2. It is a self-contained unit: it has a built-in regulation and power factor correction, 24-V dc supply with a 150-W, broadband, quartz–tungsten halogen lamp, emitting light in the region of 350–2500 nm. Light from the light source is delivered through an optical fiber (Illumination Technologies, 3mm core diameter, SMA) to the optical multiplexer [33, 40].

Figure 2.2 The light source

2.2.2 Optical multiplexer

The Fiber Optic Multiplexer (Avantes Inc. FOM-VIS-NIR (200-1100 nm), 1 x 16 channels, for 1-mm fiber core) is an instrument that can optically couple 1 input channel from the light source into 16 different output channels. The main blocks of the multiplexer are a precisely controlled stepper motor and a rotator block. Multiple COL-UV collimating lenses are used to couple the optical path. This multiplexer is controlled through a software, that comes with it and uses RS-232 protocol to interface with the computer. The software enables full control of the switching order, switching time and delay time. The device has a working

wavelength range of 350-2000 nm with a 1-mm diameter for the fiber core. There is a switching delay of 60msecs between adjacent positions [33]. I used four channels of the multiplexer for both, tissue phantom as well as animal study. Figure 2.3 shows the multiplexer used for my study.

Figure 2.3 The multiplexer

2.2.3 Spectrometer

Light from the light source is transmitted through an optical fiber to the optical multiplexer. The light transmitting fiber of the bifurcated optical fibers delivers light from the optical multiplexer output channels to the surface of the sample, and the reflected light is then collected by the detector fiber of the bifurcated optical fiber. The collected light is then delivered to one of the channels of the 8-channel CCD array spectrometer (Ocean Optics Inc, Florida, S2000 Spectrometer (350-1050 nm), and 200-µm slit width). The four sets of bifurcated fibers transmit light and collect reflected light from the sample. As discussed in the spectrometer manual, light entering the spectrometer through the entrance slit falls on a mirror that collimates the light. The collimated light strikes a diffraction grating mounted on a rotating

table. The light reflects from the grating, satisfying the conditions for interference. The light diffracted from the grating strikes a second mirror and is refocused on an exit slit. A photomultiplier tube, sensitive to the intensity of light, is mounted on the exit slit of the spectrometer [41]. The detector measures the intensity of light incident on it while the grating is rotated as shown in figure 2.4.

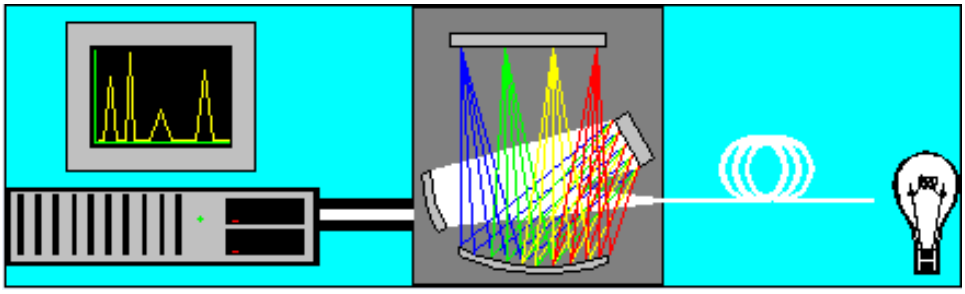

Figure 2.4 The principle of operation of the spectrometer

The S2000 is a spectrometer based on fiber optic coupling and integrated computer design. The detector in the S2000 is a CCD (charge-coupled device) array capable of measuring the intensity of light over a wide range of grating angles [41].

The detector used for the S2000 is a charge transfer device (CCD) that has a fixed well depth, capacitor associated with each photo detector, pixel [41]. As the integration time clock goes HIGH, charge transfer, reset and readout initiation begin [41]. The charge in the detector wells is transferred to a shift register for serial transfer as the integration time clock goes HIGH. This process is how the array is read. The photo detector wells are recharged to their full potential with the reset function. This allows continuous integration of the light energy during the integration time, while the data is read out through serial shift registers. Once the integration period is over, the process is repeated. The detector is considered saturated and shows the maximum output level, when a well is fully depleted by leakage through the back-biased photo

detector. The CCD is a depletion device and hence the output signal is inversely proportional to the input photons [41].

2.2.4 Optical fibers

Optical fibers in this NIRS system are bifurcated fibers. They are also called the optical needle probes, because of their small source detector separation. One fiber of each set of the bifurcated fiber, acts as a light transmitting fiber, while, the other fiber acts as a reflected light detecting fiber. The light transmitting fiber is connected to one of the 16 channels of the multiplexer, while the detecting fiber is connected to the one of the 8 channels of the multichannel spectrometer. It is desired that the light, both the transmitted and the reflected, from the bifurcated fiber, have minimum attenuation in fibers so as to achieve a highest feasible SNR. The core diameter of the optical fibers was 100 μm. The separation between source and the detector fibers for each probe was about 100 μm.

2.2.5 Data Acquisition

An optical fiber brings light from the CW light source to the input of the multiplexer. The multiplexer then multiplexes this light one at a time in each of the 16 channels. In my study, a Labview program is used for data acquisition. This program is used to acquire data from four channels of the multiplexer and to deliver the signals to the 8-channel spectrometer. As channel-1 of the multiplexer is activated, the source fiber of needle probe 1 shines light on the sample. The reflected light is collected by the detector fiber of needle probe 1. This reflected light is given to channel-1 of the 8-channel spectrometer to be stored. Once channel-1 of the spectrometer is read, the multiplexer activates the next channel, channel-2. The same steps of measurement are repeated for the multiplexer cycles through all fibers to complete one set of measurement. Spectral acquisition times are of the order of 0.5 second per channel, resulting in

a total acquisition time of 2 seconds for one set of 4 measurements. All spectra measured from the four needle probe fibers sequentially are stored in the desktop computer through the spectrometer for off-line data analysis.

CHAPTER 3

REFLECATANCE MODEL

The major chromospheres that absorb light in biological tissues are oxygenated and deoxygenated hemoglobin (HbO and Hb respectively) with distinct optical spectra in the visible and the NIR wavelength ranges.

Short source-detector separation in the optical needle probes used in this study cannot be modeled with the diffusion approximation. Such small source-detector separations in the order of 100 μm-1mm violate fundamental assumptions of the diffusion approximation as the separations are in the same order of mean free path of photons [13]. An increase of absorption coefficients as a result of hemoglobin absorption in the visible region also makes the magnitudes of absorption and scattering coefficients comparable. Hence, the diffusion model of photon transport is not valid when short source-detector separations are used as well as when visible light is employed. Many approaches have been suggested to quantify optical reflectance at short source-detector separations [9, 12, 14].

In this chapter, a broadband, steady-state, spectroscopic reflectance measurements at single short source-detector separation are used to quantify chromophore concentrations and reduced scattering coefficients of the tissues under study, using a reflectance model. This method has been used in our earlier study for the classification of prostate cancer, based on the concentrations of oxy-hemoglobin and deoxy-hemoglobin and light scattering parameters as main measures of classifications [36].

This approach uses the light reflectance measured from the sample with a very short source-detector separation; the analytical model was reported by Zonios and Dimou. The original curving-fitting program was developed by Dr. Dheerendra Kashyap, a former group member. It uses the ant colony optimization algorithm to quantify concentrations of oxy-hemoglobin and deoxy-hemoglobin. To further improve the accuracy of this method and to find an appropriate set of the optical needle probes for my study, I have to validate the analytical model by calibrating the system parameters through a series of rigorous phantom measurements. Once the phantom analyses are known to be positive, this method is used for the pain study.

3.1 Reflectance Model for short source-detector needle probes

Optical needles probes with short source-detector separation are used in my study. Zonios and Dimou presented a model to quantify and relate the optical reflectance measured with optical probes having short source-detector separations to the reduced scattering coefficients and absorption coefficients of the medium [12]. The semi-empirical model by Zonios and Dimou is shown in Equation (3.1) as follows [12]:

$$R_p(\lambda) = \frac{1}{k_1 \frac{1}{\mu_s'(\lambda)} + k_2 \frac{\mu_a(\lambda)}{\mu_s'(\lambda)}} \tag{3.1}$$

where $R_p(\lambda)$ is the optical reflectance measured by the optical probe at a particular measurement wavelength λ, k_1 and k_2 are parameters depending on geometrical characteristics of the optical probe, $\mu_s'(\lambda)$ is the reduced scattering coefficient, and $\mu_a(\lambda)$ is the absorption coefficient at wavelength λ.

For a probe to be used in any particular study, its k_1 and k_2 values need to be calibrated experimentally using tissue phantoms. The k_1 and k_2 values are specific to a particular probe and

detection system. Absorption coefficients are functions of deoxygenated hemoglobin concentration *[Hb]*, oxygenated hemoglobin concentration *[HbO]*, melanin concentration, C_{mel}, and water fraction, as described in Equations (3.2) and (3.3).

The spectral dependence of $\mu_a(\lambda)$ for blood-perfused tissues can be written as

$$\mu_a(\lambda) = [HbO]\varepsilon_{HbO}(\lambda) + [Hb]\varepsilon_{Hb}(\lambda) + \varepsilon_{H_2O}\%H_2O + [C_{mel}]\varepsilon_{mel}(\lambda) \tag{3.2}$$

where λ is the wavelength in nanometers; $\varepsilon_{HbO}(\lambda)$, $\varepsilon_{Hb}(\lambda)$, and $\varepsilon_{H_2O}(\lambda)$ are extinction coefficients of HbO, Hb and water, respectively. The spectral dependence of $\mu_s'(\lambda)$ can be approximately written as

$$\mu_S'(\lambda) = \left(1 - \frac{d_0^{1/2}}{d_S^{1/2}} \frac{\lambda - \lambda_{\min}}{\lambda_{\max} - \lambda_{\min}}\right) \mu_S'(\lambda_{\min}) \tag{3.3}$$

,

where the maximum and minimum wavelengths were originally selected as λ_{max}=850 nm and λ_{min}=500 nm, respectively, d_S represents the effective scatterer size, and d_0 is a constant and equals 0.0625 μm. Equation (3.3) describes a linear dependence of reduced scattering coefficients on the wavelength. It can be seen that it is a reasonable approximation of the Mie theory for spherical scatterers, as given by Flock et al [16]. As observed from the above equation, the maximum and minimum λ have been considered in accordance with the visible and the near infrared window of the light spectrum.

3.2 Forward Calculation

Forward calculation is basically calculation of k_1 and k_2 specific for a probe. The k_1 and k_2 are calculated from phantom experiments. These phantoms are blood-intralipid phantoms to replicate tissue. The phantom experiments are explained in details in section 3.4.

3.2.1 Calculation of absorption and reduced scattering coefficients

Absorption coefficients at all wavelengths in the visible and NIR range were calculated from the measured blood hemoglobin concentrations and published hemoglobin extinction coefficients [37]. The extinction coefficients for HbO and Hb are obtained from Scott Prahl's compilation. During the calibration process the absorption coefficients (μ_a) are obtained from the ISS Oximeter at 730 nm and 850 nm. To calculate the Hb and HbO concentration in μM from the values of μ_a the following equations were used:

$$HbO_2 = ((\mu_{a750}*\varepsilon_{Hb830})-(\mu_{a830}*\varepsilon_{Hb750})) / (\varepsilon_{HbO2\,750}*\varepsilon_{Hb830} - \varepsilon_{HbO2\,830}*\varepsilon_{Hb750})*1000; \quad (3.4)$$

$$Hb = -((\mu_{a750}*\varepsilon_{HbO2\,830})-(\mu_{a830}*\varepsilon_{HbO2\,750}))/(\varepsilon_{HbO2\,750}*\varepsilon_{Hb830} - \varepsilon_{HbO2\,830}*\varepsilon_{Hb750})*1000;$$

After obtaining the Hb and HbO concentrations, the range of μ_a for the respective wavelengths was found. The equation used to calculate the range of μ_a was:

$$\mu_a(\lambda) = [HbO_2] * \varepsilon_{HbO2}(\lambda) + [Hb] * \varepsilon_{Hb}(\lambda) \quad (3.5)$$

Thus using the above set of equations the entire range of the respective μ_a were calculated for the different blood concentrations.

For calculating μ_s', two models were used. The first model used for the calculation of μ_s' is Mie theory model published by Staveren et al. The equation for calculating μ_s' for 10% of Intralipid solution is:

$$\mu_s = (2.54 \times 10^{9})(\lambda^{-2.4})\ [cm^{-1}] \quad (3.6)$$

$$g = 1.1 - (0.58 \times 10^{-3})*(\lambda) \quad (3.7)$$

$$\mu_s' = \mu_s(1-g) \quad (3.8)$$

Thus, using the above equations, the reduced scattering coefficient is approximated. For calculating the μ_s' range for respective calibration, intralipid concentration is calculated as follows:

We assume x% concentration of intralipid and have

$$\mu_s' (750nm)_x = A$$

$$\mu_s' (830nm)_x = B$$

A & B are obtained from the ISS Oximeter during the experiment calibration procedure. Then, using equations 3.6, 3.7 and 3.8, μ_s' values at wavelengths 750 nm and 830 nm can be calculated as $\mu_s'_{750nm}$ and $\mu_s'_{830nm}$. Now that we know the μ_s' values for x% intralipid as well as at 10% intralipid, dividing the two values, we would get scaling factors C and D as shown below.

$$C = \frac{\mu_s'_{750nm}}{A}$$

$$D = \frac{\mu_s'_{830nm}}{B}$$

To calculate the $\mu_s'(\lambda)$ for x% intralipid, the average of the two scaling factors, C and D, is calculated. Then, $\mu_s'(\lambda)$ values for 10% intralipid are divided by the scaling. Thus we can obtain the $\mu_s'(\lambda)$ at x% intralipid solution.

The second model used for μ_s' calculation is the linear model. This is a relatively simpler model as compared to the Mie theory model. For $\mu_s'(\lambda)$ at x% intralipid concentration, the μ_s' at two wavelengths, 750 nm and 830 nm, have been obtained from the ISS oximeter.

$$\mu_s' (750nm)_x = A$$

$$\mu_s' (830nm)_x = B$$

Using scatter plots, A and B are then plotted against wavelength. The slope and intercept are calculated using a linear fit. The $\mu_s'(\lambda)$ for x% intralipid can be determined using a linear curve fitting, as given in equation 3.9.

$$\mu_s'(\lambda) = \text{intercept} + (\text{slope}) * \lambda \tag{3.9}$$

3.2.2 Determination of k_1 and k_2

The parameters of k_1 and k_2 in Equation (3.1) are determined using the least squares approach by using Moore-Penrose pseudo inverse. Equation (3.1) can be rewritten as

$$\frac{\mu_s'(\lambda)}{R_p(\lambda)} = k_1 + k_2 \mu_a(\lambda) \quad , \tag{3.10}$$

Equation (3.10) is valid for every wavelength in the spectrum. From the explanations given earlier and equation (3.10), we know $\mu_s'(\lambda)$, $\mu_a'(\lambda)$ and R_P.

After plotting $\frac{\mu_s'(\lambda)}{R_p(\lambda)}$ versus $\mu_a'(\lambda)$, we get a linear line where its slope is k_2 and the intercept is k_1.

3.3 Inverse calculations

The inverse calculation deals with determination of tissue chromophore ([HbO] and [Hb]) concentrations and scattering coefficients from measurements of diffuse reflectance on the tissue surface. The k_1 and k_2 values were calculated experimentally, with a blood intralipid phantom as explained earlier in this chapter. The algorithm calculates a set of values for oxy-hemoglobin and deoxy-hemoglobin concentrations and scattering coefficients from the given solution space that best fit the measurement of spectral diffuse reflectance using least squares analysis. It can be expressed as follows:

$$\chi^2 = \sum_{i=1}^{M} \left[R_p(\lambda_i)^{(measured)} - R_p(\lambda_i)^{(predicted)} \right]^2 \tag{3.11}$$

where M is the number of wavelengths, $R_p(\lambda_i)^{(measured)}$ and $R_p(\lambda_i)^{(predicted)}$ are the reflectance values measured by the thin optical probe and calculated by using the prediction of hemoglobin concentrations and scattering coefficients selected from the optimization algorithm at wavelength λ_i.

3.4 Phantom Studies

3.4.1 Experimental setup for tissue phantoms

Tissue phantoms were prepared using intralipid (Baxter Healthcare Corporation, Deerfield, IL) and hemoglobin from horse blood (Hemostat Inc, San Francisco, CA). The blood and intralipid were diluted with Phosphor Buffer Saline (PBS) solution. PBS was used to maintain the blood pH at ~7 in the blood intralipid phantom. An intralipid solution is a very good choice for a tissue phantom as it closely resembles the light scattering properties of tissue with an estimated g (cosine of mean scattering angle) > 0.9 and a mean particle size of 0.5 μm [17].

A rectangular plastic container with dimensions of 10 cm x 8 cm x 14 cm (height x width x length) as shown in Figure 3.1 was used to hold the testing intralipid solution. The probes were inserted from the top into the solution during the measurement, so there was no intralipid-container or intralipid-air interface for the probe. The thin probe tip was faced vertically down towards the bottom of the container, 2-3 cm below the solution surface, and 4-5 cm away from the walls of the container. Integration times of spectral acquisition were so adjusted to prevent saturation of the CCD detector. The lowest integration time for measurement was chosen to ensure that measured intensities were greater than 500 counts [8]. ISS Oximeter (ISS Inc, Champaign, IL) and the thin optical fiber probe [8, 15] were used for simultaneous measurements the blood intralipid phantom. The ISS Oximeter gives us a measure

of reduced scattering coefficients and HbO and Hb concentrations at two wavelengths, 750nm and 830nm. Optical reflectance in the visible and NIR wavelength range was measured using our optical probe [9].

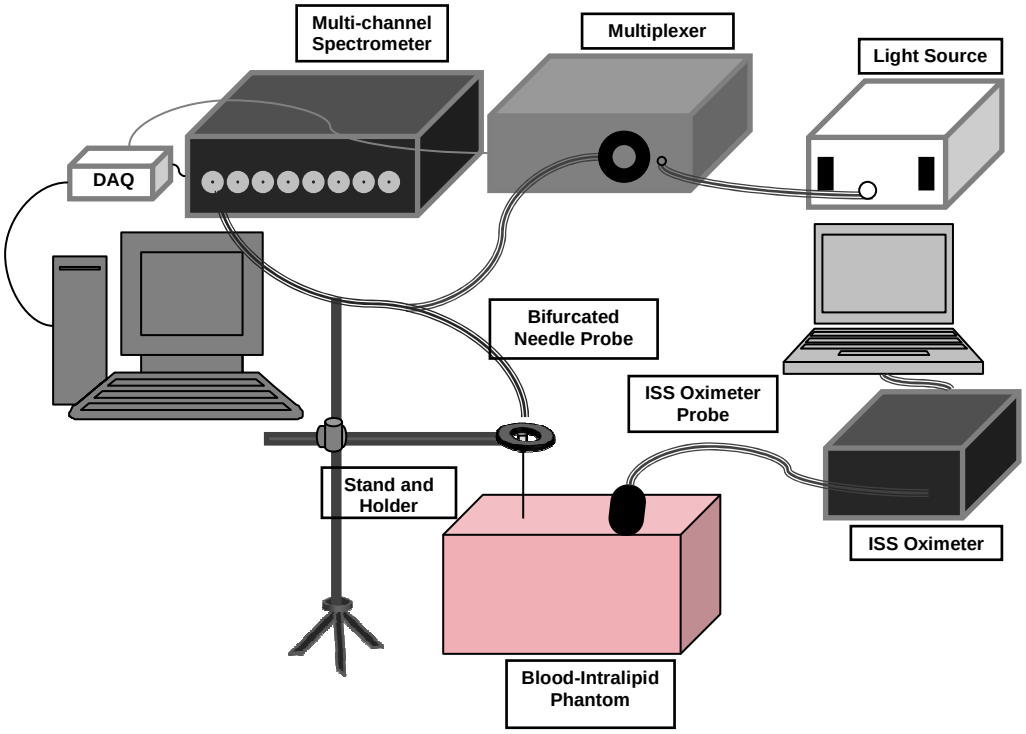

Figure 3.1 Schematic diagram of phantom, illustrating positions of the thin fiber probe and ISS Oximeter probe. The thin probe tip was facing vertically down, 2-3 cm below the solution surface, and 4-5 cm away from the walls of the container. The probe position of ISS oximeter is also shown.

The Intralipid stock solution was 20% by volume, and the diluted Intralipid solutions ranged in concentration from 0.5%-2.0%, depending on the reduced scattering coefficient desired. In general, the reduced scattering coefficients, μ_s', found in tissues vary between 5 and 25 cm^{-1}; however, larger values of μ_s' have been reported in brain tissues [34, 35]. The reflectance measurements from the optical probes were calibrated using the reflectance from the same optical probe on a standard reflectance white sample (WS-1, Ocean Optics, Dunedin, FL,

USA). This standard sample has a reflectance of almost 100% throughout the wavelength range (350-1100nm) [36].

Two phantom experiments were conducted. In one phantom experiment, the reflectance spectra were taken at different Intralipid concentrations and different blood concentrations (as listed in Table 3.1) from one of the probes. Each set of data, for example, at one particular intralipid and blood concentration, gave us reflectance spectra. The $\mu_s'(\lambda)$ and $\mu_a'(\lambda)$ were calculated from equations (3.5) and (3.8), based on which μ_s' model was used (Linear or Mie theory). μ_s' values at wavelengths of 750 nm and 830 nm and HbO and Hb concentrations were obtained from the ISS Oximeter.

Table 3.1 The different blood and intralipid concentrations used in the phantom study, as well as the k_1 and k_2 for each condition.

	K1	K2
20uM Blood_1%intralipid	17.08	2.02
25uM Blood_1%intralipid	17.19	2.27
30uM Blood_1%intralipid	17.21	2.49
35uM Blood_1%intralipid	17.39	2.50
20uM Blood_1.5%intralipid	15.63	2.11
25uM Blood_1.5%intralipid	15.66	2.22
30uM Blood_1.5%intralipid	15.72	2.15
35uM Blood_1.5%intralipid	15.98	2.05
20uM Blood_2%intralipid	15.07	2.11
25uM Blood_2%intralipid	14.87	2.63
30uM Blood_2%intralipid	14.88	2.27
35uM Blood_2%intralipid	15.17	2.64
Average	**15.99**	**2.29**
Stdev	0.97	0.22
Percentage Stdev	6.08	9.74

Once all the parameters of the equation (3.10) are calculated, (Rp/μ_s') versus the μ_a' (λ), was plotted. A linear line was fit for the data and k_1 and k_2 were the intercept and the slope, respectively, as shown in Figure 3.2. The k_1 and k_2 values from the different set of data were averaged to get one value, which would be specific to the probe, for further studies.

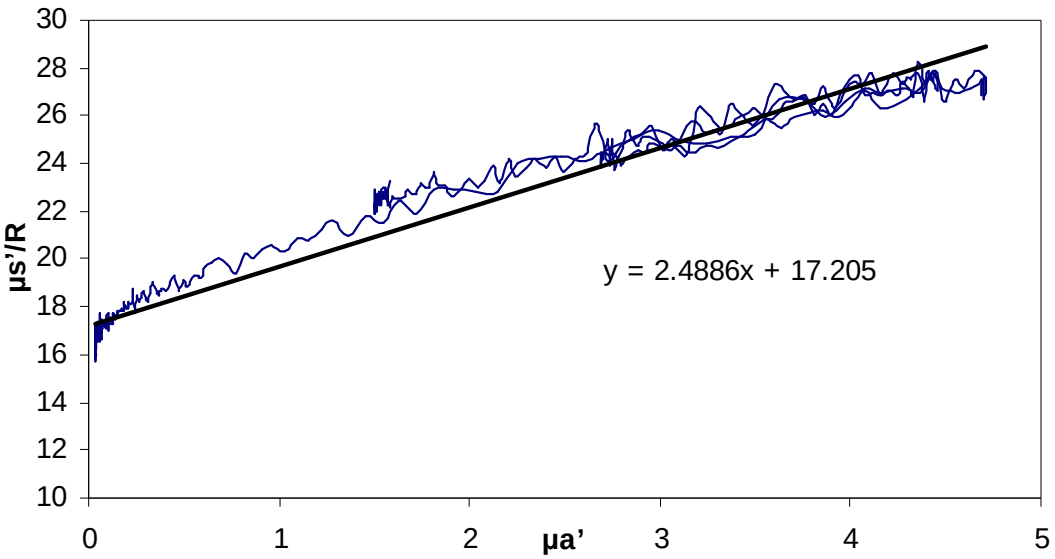

Figure 3.2 The scatter plot for (Rp/μ_s') versus μ_a' (λ), k_1 and k_2 and are the intercept and the slope, respectively

Another set of phantom studies were performed to validate the reflectance model at different blood oxygenation. In this experiment, one intralipid and blood concentration, diluted with PBS, was used. This concentration was kept the same throughout the experiment. ISS oximeter and the optical probe were used to simultaneously measure the blood-intralipid phantom. 4-5grams of yeast were added in the phantom of a total volume of 3000 ml. After 10-15mins, the yeast started consuming oxygen in the hemoglobin. Continuous and simultaneous measurements were taken from both the ISS oximeter and optical probe. The optical probe measured the reflectance from the phantom, whereas the ISS oximeter provided the values of

HbO, Hb, HbT, and μ_s'. As the yeast kept consuming oxygen from the hemoglobin in blood, the blood oxygen level decreased and data was collected at certain blood oxygenation levels. After the lowest blood oxygenation was seen, oxygen gas was pumped into the phantom. As oxygen was pumped, the blood oxygenation level increased. Data was collected at certain increasing blood oxygenation levels. The $\mu_s'(\lambda)$, $\mu_a(\lambda)$, and light scattering are calculated as discussed earlier.

3.5 Beer-Lambert's Law

Another method for quantitative data analysis is used to measure relative changes in HbO and Hb concentrations using Beer-Lambert's law. This method is faster as compared to the fitting method discussed earlier, but it gives us only the relative changes in both HbO and Hb concentration. Beer Lambert's law expresses light absorption as a function of hemoglobin concentration as given [20] [21].

$$OD = \text{Log}(I_0/I) = \varepsilon c L \tag{3.12}$$

where OD is the optical density, I_0 is the light intensity of incident light, I is the light intensity of transmitted light, ε is the extinction coefficient of hemoglobin, *c* is the concentration of hemoglobin, and *L* is the length of light path through solution.

Blood hemoglobin concentration, *c*, can be expressed as a combination of oxy-hemoglobin and deoxy-hemoglobin. As shown in the equation given below [20] [21],

$$OD^{\lambda} = \{\varepsilon_{Hb}{}^{\lambda} [Hb] + \varepsilon_{HbO2}{}^{\lambda} [HbO_2]\} L, \tag{3.13}$$

where OD (λ) is the optical density or absorbance at wavelength λ, $\varepsilon_{Hb}(\lambda)$ and $\varepsilon_{HbO2}(\lambda)$ are the extinction coefficients at wavelength λ for molar concentrations of deoxygenated hemoglobin ([Hb]) and oxygenated hemoglobin ([HbO_2]), respectively.

By employing two wavelengths, 500 nm and 600 nm, and measuring the light reflectance at the two specific wavelengths, using Equation (3.13), both of [HbO_2] and [Hb] can be solved, as given below, since we already know the values for $\varepsilon_{Hb}(\lambda)$ and $\varepsilon_{HbO2}(\lambda)$.

$$[\text{HbO2}] = \frac{\varepsilon_{Hb}^{\lambda_2} OD^{\lambda_1} - \varepsilon_{Hb}^{\lambda_1} OD^{\lambda_2}}{L\left(\varepsilon_{Hb}^{\lambda_2}\varepsilon_{HbO_2}^{\lambda_1} - \varepsilon_{Hb}^{\lambda_1}\varepsilon_{HbO_2}^{\lambda_2}\right)}$$

$$[\text{Hb}] = \frac{\varepsilon_{HbO_2}^{\lambda_2} OD^{\lambda_1} - \varepsilon_{HbO_2}^{\lambda_1} OD^{\lambda_2}}{L\left(\varepsilon_{Hb}^{\lambda_1}\varepsilon_{HbO_2}^{\lambda_2} - \varepsilon_{Hb}^{\lambda_2}\varepsilon_{HbO_2}^{\lambda_1}\right)}$$

$$\Delta[\text{HbO2}] = \frac{\varepsilon_{Hb}^{\lambda_2} \Delta OD^{\lambda_1} - \varepsilon_{Hb}^{\lambda_1} \Delta OD^{\lambda_2}}{L\left(\varepsilon_{Hb}^{\lambda_2}\varepsilon_{HbO_2}^{\lambda_1} - \varepsilon_{Hb}^{\lambda_1}\varepsilon_{HbO_2}^{\lambda_2}\right)}$$

$$\Delta[\text{Hb}] = \frac{\varepsilon_{HbO_2}^{\lambda_2} \Delta OD^{\lambda_1} - \varepsilon_{HbO_2}^{\lambda_1} \Delta OD^{\lambda_2}}{L\left(\varepsilon_{Hb}^{\lambda_1}\varepsilon_{HbO_2}^{\lambda_2} - \varepsilon_{Hb}^{\lambda_2}\varepsilon_{HbO_2}^{\lambda_1}\right)}$$

where ΔOD^{λ} represents a change in optical density at the specific wavelength, λ, and equals log (A_B/A_T). A_B and A_T correspond to light intensities measured under the baseline and transient conditions.

The data obtained during the yeast measurements, as explained earlier, were used to validate the method using Beer-Lambert's law. In this case, the blood oxygen level before adding yeast was considered as the baseline. The period after the addition of the yeast was considered the transient period. Hence the output of this data would show the change in oxy-hemoglobin and deoxy-hemoglobin with respect to the baseline, as shown in Figure 3.3.

To understand the effects of change in scattering medium on the accuracy of determination in HbO and Hb, another experiment was performed. In this experiment, the blood concentration was kept constant at 30µM and the intralipid concentration was increased from 1% to 5%. Here, reflectance data at 1% intralipid concentration was considered as the baseline; all other concentrations of intralipid were considered in the transient conditions and hence the change in absorbance was shown with respect to the baseline, as shown in Figure 3.4. This figure shows that the change in oxy-hemoglobin is almost zero, whereas the change in deoxy-hemoglobin is dependent on the change in scattering. Hence, using Beer-Lambert's law, it is difficult to differentiate the effects between the actual change in deoxy-hemoglobin concentration and the change in scattering. But, this relative method can provide us with a fast and relatively accurate means to quantify changes in oxy-hemoglobin concentrations.

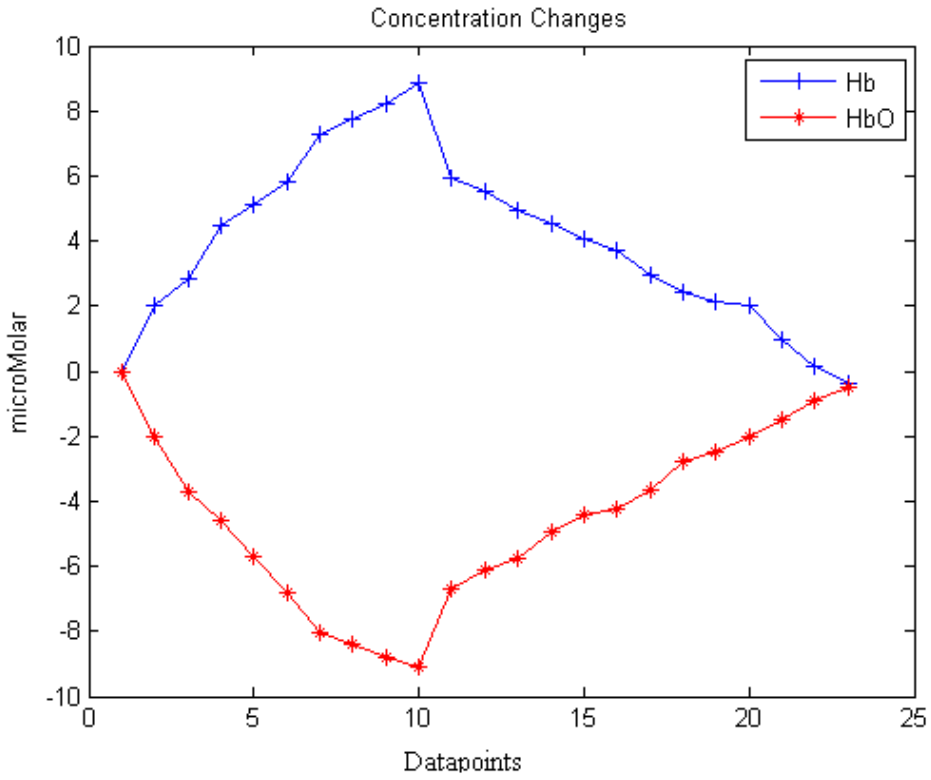

Figure 3.3 The change in [HbO] and [Hb] during yeast measurements and pumping of oxygen

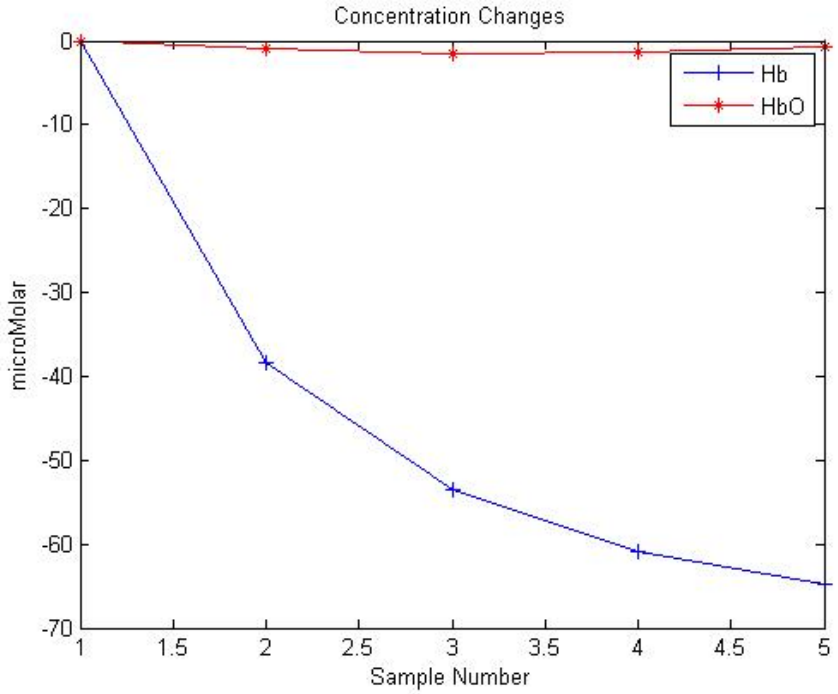

Figure 3.4 The effect of increasing intralipid concentration on the change in the [HbO] and [Hb] keeping blood concentration constant.

3.6 Look -Ahead Distance (LAD)

When I first started using the optical spectroscopic system, as explained in Chapter 2, for pain study in rats, I used an optical needle probe with a source-detector separation of 700 µm. The animal pain study and its protocols are to be explained in details in Chapter 4. This study was planned to monitor the hemodynamic changes over the spinal cord, which is exposed through laminectomy, and also the changes at the brain due to peripheral stimulations. When the 700-µm optical probes were used to measure signals on the spinal cord, no signal changes were detected. This led to the quantification of the Look ahead distance of the probe. The look ahead distance (LAD) basically is the largest or farthest distance at which the target sample is "seen" or "detected" by the optical needle probe above it.

A phantom experiment was carried out to measure the LAD of the probe. In this phantom study, two probes were used: one with source-detector separation of 700 µm and the other with 100µm [25]. A plastic capillary of 3 mm diameter, covered with a black tape, was used as a sample, possibly resembling the spinal cord. The phantom was made from intralipid solution mixed with PBS and 30-µM blood, and the intralipid concentration was 2% of the total solution of 3000ml. The probes were held orthogonal to the horizontal plane, at a distance of 1mm from each other. This probe set up was held with the help of a probe holder. A black thin plate covered a large area of the rectangular container and was held horizontally by a vernier height gage, which had the precision of 0.2 mm vertical movement. The experimental diagram is shown in Figure 3.5. This black plate was kept below the two optical probes under testing. This set up was immersed in the phantom solution. The horizontal black plate was then moved in an interval of 1 mm from right below the probe tips to 25 mm below the tips while the data were collected at each depth.

The data was analyzed empirically; the slope of the reflectance curve from 700 nm to 850 nm was calculated [25]. These slopes were plotted against the increasing distance between the probes and the black plate, as shown in Figure 3.6. It is seen from Figure 3.6 that the LAD for the probe with source-detector separation of 100 µm is between 3 mm to 5 mm, and that of the 700-µm source-detector separation is between 7 mm to 9 mm. This shows that the probe with 700-µm source-detector separation would detect signals from tissues that are 7 mm to 9 mm deep. This explains why we did not obtain good results in the earlier animal study since those 700-µm probes detected the signal changes from a deeper tissue volume than those on the spinal cord, which is approximately 3 mm in diameter. More accurately, the signal changes due to peripheral stimulations seen by the 700-µm source-detector separation probe are averaged over the entire 7-mm deep volume, not only specific from the spinal cord. Hence, shifting to the

100-µm source-detector separation probes was advised, as the LAD was 3 mm to 5 mm, optimal for the detection of signals from the spinal cord only.

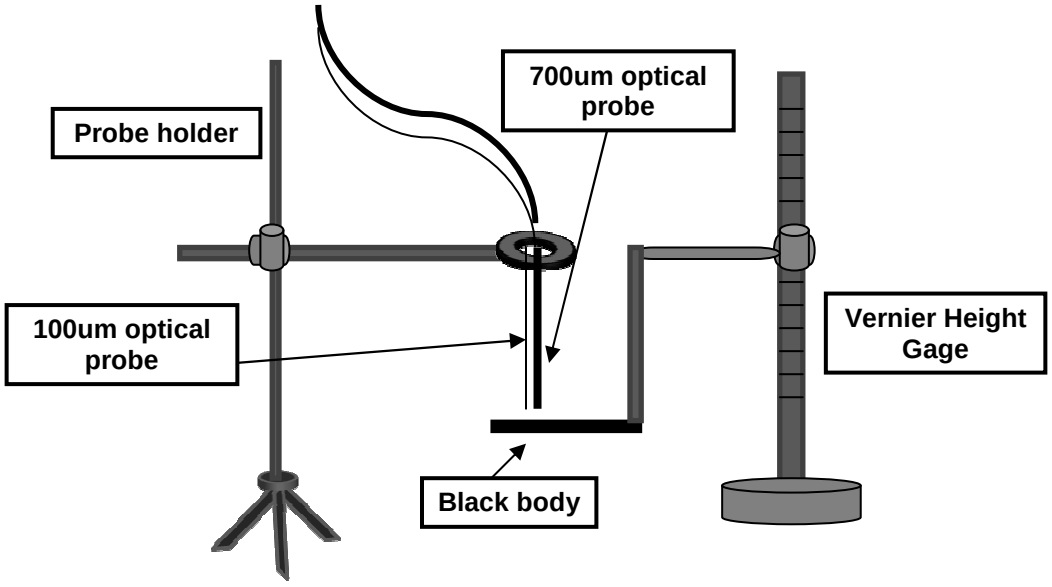

Figure 3.5 The schematic diagram of the experimental set up to determine the LAD of the probes of 700um and 100um source-detector separation. The above set up is immersed in a intralipid phantom

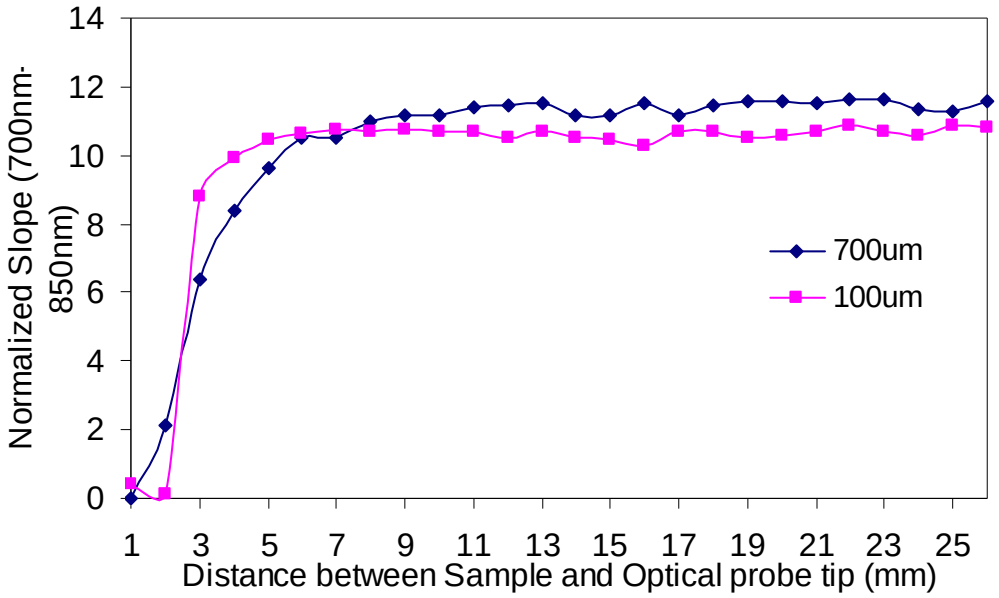

Figure 3.6 The experimental results of normalized slope versus the distance between the probes and the black capillary.

CHAPTER 4

PAIN STUDY

4.1 Introduction

Noxious peripheral stimulations cause changes in peripheral circulation. Previously, performed investigations to characterize peripheral blood flow changes, due to pain stimulations, have been to quantify relative changes with respect to the baseline. In this study, changes in peripheral circulation as a result of electrical stimulations are quantified with spectral alterations in optical signals. The quantifications are not limited to change in relative units, rather elicit changes in oxygen saturations, increase of oxygenated and total hemoglobin concentrations. Optical reflectance signals were measured simultaneously on the brain and the spinal cord, while the hind paw of the anesthetized rat was stimulated electrically. The temporal evolutions of signal changes during and after the stimulations were monitored by a multi-channel spectrometer. The mathematical model [12] and Modified Beer Lambert's Law, explained in Chapter 3, were used for this study; the result show significant increases in oxygenated hemoglobin concentrations induced by the noxious stimulation, electrical stimulations, were detected in the ipsilateral side of the spinal cord and the contralateral side of the S1 region of the brain.

4.2 Animal preparation and experimental protocols

The animal preparation and animal measurement were carried by Dr. Yuanbo Peng's student, Mr. Ji Wei He, from the Department of Psychology at UT Arlington. My major responsibility for this research project was to setup the instrument, assure good contacts between the probes and animals, acquire data continuously during and after delivering

stimulations, perform data analysis, and interpret the data that were obtained under the electrical stimulation of 10 V.

Adult male Sprague Dawley rats were initially anesthetized with pentobarbital (50 mg/ kg, i.p.). Laminectomy was performed on the rat to expose thoracic and lumbar regions of the spinal cord for proper placements of the optical probes on the spinal cord. The scalp over the somatosensory region in the brain was also removed for better placement and contact of optical probes on the brain. The Somatosensory region was identified using the rat brain atlas. Mineral oil was used to prevent the drying of the exposed surface. A catheter was placed into the jugular vein for continuous administration of anesthesia. Musculature paralysis was achieved by an intravenous placing of an injection of 1 ml pancuronium delivered in 1 minute. Controlled ventilation was administered through a tracheal cannula following tracheostomy. Continuous anesthesia was accomplished by administering intravenous injection of pentobarbital of 5mg/ml at a rate of 0.02 ml per minute. The end tidal CO_2 was maintained at around 30 mmHg. The animal's body temperature was maintained at 37.8°C by a feedback controlled electric heating blanket. The experimental setup and arrangements of optical probes for the study are shown in Figure 4.1. Rat was held in a stereotaxic frame to prevent movement during recording. Four calibrated optical probes were used for the study of pain stimulation in the hind paw. Two probes were placed on the spinal cord, on both sides, and two on the brain in the somatosensory region, on both sides. The probes were held in a stable position with the help of probe holders attached to the stereotaxic frame. The probes were placed in a vertically straight position, in a way that, it just touches the tissue under study. Care was taken such that the probes do not put pressure on the tissue, which would disturb the absorption and scattering parameters of the tissue. Adequate support was provided to facilitate placements of the optical probes and a stable

system was achieved. Any artifacts due to movements of the probes were minimized due to the stable system.

A ball electrode was used to locate the lumbar region of the spinal cord, to achieve better signals for the optical needle probes during stimulations [24]. The ball electrode was first placed on the spinal cord region, prior to the actual placements of the optical probes; another electrode was pinned in the fore paw. Gentle stimulations using a brush were given on the hind paw of the rat. The ball electrode catches the action potentials and a system converts these signals into sound signals. The ball electrode was moved over the spinal cord to achieve the largest response signal. This region was considered the lumbar region of the spinal cord. The area was visually marked and the ball electrode was removed. Optical needle probes were then placed in the marked area. Data acquisition system was as explained in section 2.2.

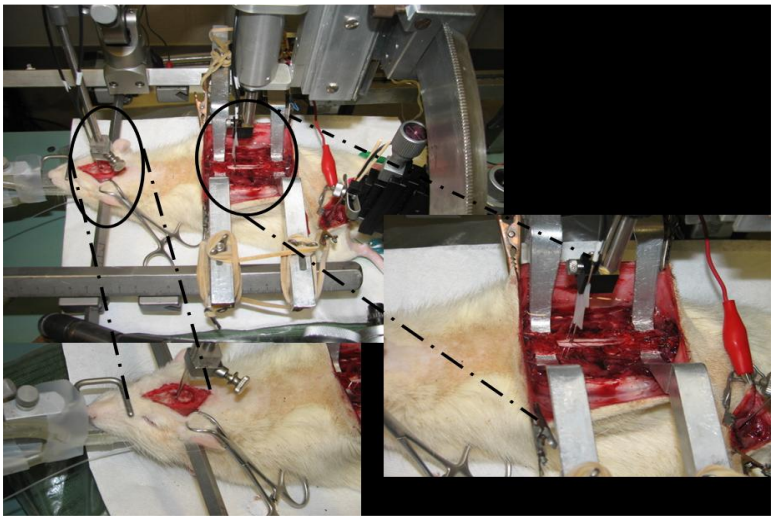

Figure 4.1 The experimental set up and the probe placement on the brain and spinal cord

4.2.1 Baseline measurements

After completing all preliminary animal preparations, baseline measurements of reflectance spectra were made for two minutes. The measurements were made only after the eye blink and tail pinch responses of the rat were eliminated. Measurements were made with a

sampling time of 2 second. All measurements were made in dark surroundings to eliminate ambient light contamination. To eliminate any contribution of ambient light, dark signals were measured and subtracted in post data analysis. Vital signs were monitored throughout the experiment. The data acquisition system, simultaneously, measured data at four locations of the probe placement.

4.2.2 Stimulations

After two minutes of baseline measurements, electrical stimulations were given on the plantar surface of the hind paw. Electrical stimulation protocol included delivering electrical stimulations to the plantar paw of the same hind limb. The Electrical stimulations were with a graded intensity from 5 V to 15 V stimulations, in a consecutive increment of 5 V, at a frequency of 10 Hz and pulse-width of 1 ms duration. The stimulations were given for 10 s. The inter-stimulus interval (ISI) was about two minutes. Five block stimulations were performed, at each electrical intensity. As the rat was paralyzed, care was taken to ensure that there was no movement of optical probes at any location.

All procedures used in this study were approved by the Animal Care and Use Committee of UTA and followed guidelines for treatment of animals of the International Association for the Study of Pain.

4.3 Data Analysis

Once the data was collected on both, the ipsilateral and contralateral side, at the brain and spinal cord, during and after stimulating the rat paw, this data was then processed using the reflectance model explained in details in Chapter 3. In my study, I analyzed the data taken only from 10V electrical stimulations in order to demonstrate the usefulness of the method. More complete and thorough analysis can be found in Mr. Ji Wei He's future dissertation. Equation 3.10 shows a mathematical relation between reflectance, $R_p(\lambda)$, coefficient of absorption, μ_a, and

reduced coefficient of scattering, μ_s'. In this equation, k_1 and k_2 are parameters depending on geometrical characteristics of the optical probe and were determined experimentally using tissue like blood-intralipid phantoms as explained in Chapter 3. The set of k_1 and k_2 for the optical probes used in this study have been tabulated in Table 4.1. The $R_p(\lambda)$ in equation 3.10 was the measured reflectance from the spinal cord and brain. [*HbO*], [*Hb*] and [Hb_{Total}] and scattering parameters can be determined from equation 3.10 after k_1 and k_2 were fully calibrated.

Table 4.1 The k_1 *and* k_2 values used in the pain study

Probe	K1	K2
#2	19.57944	2.869189
#3	14.1786	1.941544
#4	16.8612	2.467233
#5	15.98625	2.344833

The values of [*HbO*], [*Hb*] and [Hb_{Total}] and μ_s' were then plotted against time. Detrending of data was carried out wherever necessary. As I have a blocked design for each of the stimulations, the block average needs to be analyzed. The 10 seconds of baseline data, 10 seconds of stimulation period and 40 seconds of the recovery time were grouped together for each of the stimulations, on all rats. [*HbO*], [*Hb*] and [Hb_{Total}] and μ_s' during the baseline were subtracted from the entire 50 seconds data (10 seconds of stimulation and 40 seconds of recovery time). Hence, I quantified the changes in [*HbO*], [*Hb*] and [Hb_{Total}] and μ_s' during and after stimulation.

To analyze the blocked design, I preformed one way ANOVA on each of the five blocks, for all stimulations, for each rat. This was performed in MATLAB, to compare the means of each of the five blocks of data, where each block was considered an independent sample containing mutually independent observations. It evaluates the hypothesis that the five

blocks, all have the same mean against the alternative that the means are not all the same. Another command ‘multcompare’ was used to perform a multiple comparison test; it returned a matrix of pair-wise comparison results between each of the five blocks. Each row of this matrix represented one test, and there contained one row for each pair amongst the five blocks. The entries in the row indicated the means of the two blocks being compared, the estimated difference in means, and a confidence interval for the difference. If the confidence interval did not contain zero, the pair was considered significantly different and vice versa. The block that was significantly different from others was removed for further analysis, as shown in Figure 4.2.

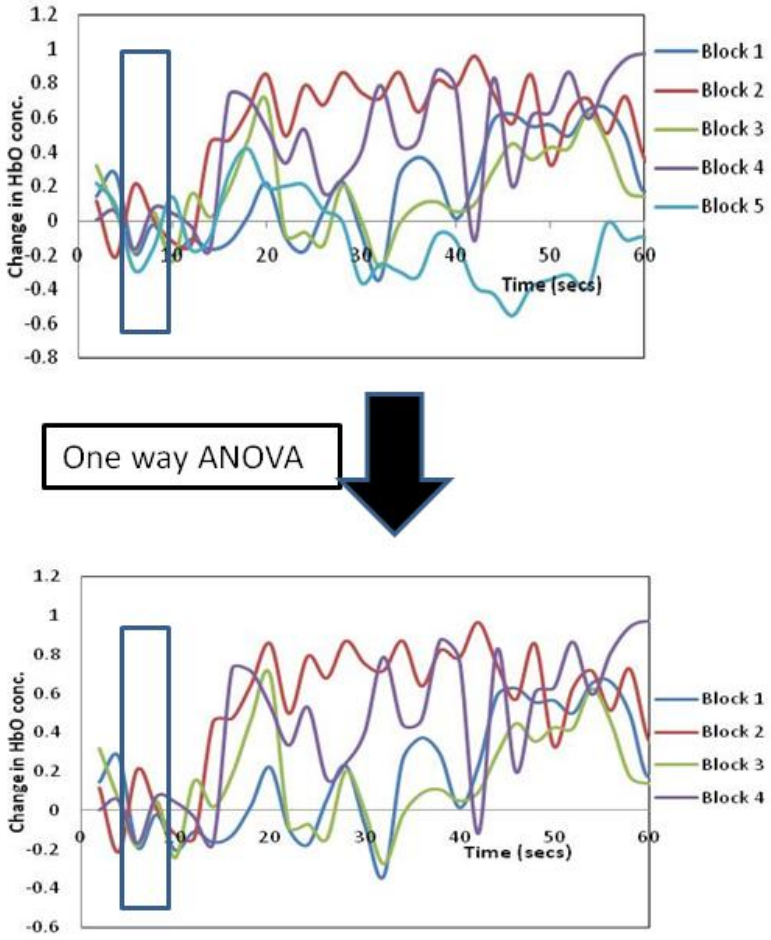

Figure 4.2 The use of one way ANOVA in analyzing block design

Figure 4.2 shows the change in [*HbO*] at the contralateral side of the brain due to electrical stimulations on the paw. It can be seen and also statistically proved that block 5 was different from the other blocks. The probable reason for seeing difference in the blocks with the same stimulations could be due to the change in physiology of the rat caused by repeated stimulation on the same region. This set of data was then block averaged over the remaining blocks for each of the stimulations.

The block averages for changes in [*HbO*], [*Hb*] and μ_s' for the 10 V electrical stimulations are shown in section 4.4. For further analysis, to see if the changes in [*HbO*], [*Hb*] and μ_s' were significant over all rats, I performed the mixed design ANOVA analysis.

In this type of analysis, using the mixed model, there were two groups. One group was within subject variability and second was between subject variability. Within subject, I had two groups, one during baseline and one during and after stimulation. Using the mixed model ANOVA, I checked if there was significant change in [*HbO*], [*Hb*] and μ_s' during and after stimulation as compared from the baseline, over all rats. This model would give a p-value which would tell if there was significant difference. This p-value was over all rats to show if there was any significant difference between the two groups.

4.4 Result and Discussion

4.4.1 Spinal cord

Data was analyzed as explained in section 4.3. Change in [HbO] and [Hb] was analyzed separately. Figure 4.3 shows the change in [HbO] at the ipsilateral side of the spinal cord due to 10 V, 10 Hz electrical stimulations with 1ms pulse width on the paw. They are block averaged temporal profiles for 10 rats. Figure 4.4 shows the change in [Hb] at the spinal cord, induced by the same 10 V electrical stimulations.

It is seen that there was an increase in [HbO] and a decrease in [Hb] from the baseline, during and after stimulations. Neuronal activity leads to different physiological events, which may result in local increase in blood flow, increase in blood volume and also an increase in metabolic rate of vascular oxygen, all of which are termed as 'the hemodynamic response' [28]. Our experimental results may well demonstrate an obvious alteration in hemodynamic response caused by electrical stimulation. Specifically, it is seen that all ten rats showed significant changes in [HbO] due to electrical stimulation of 10V, 10Hz and 1ms pulse width.

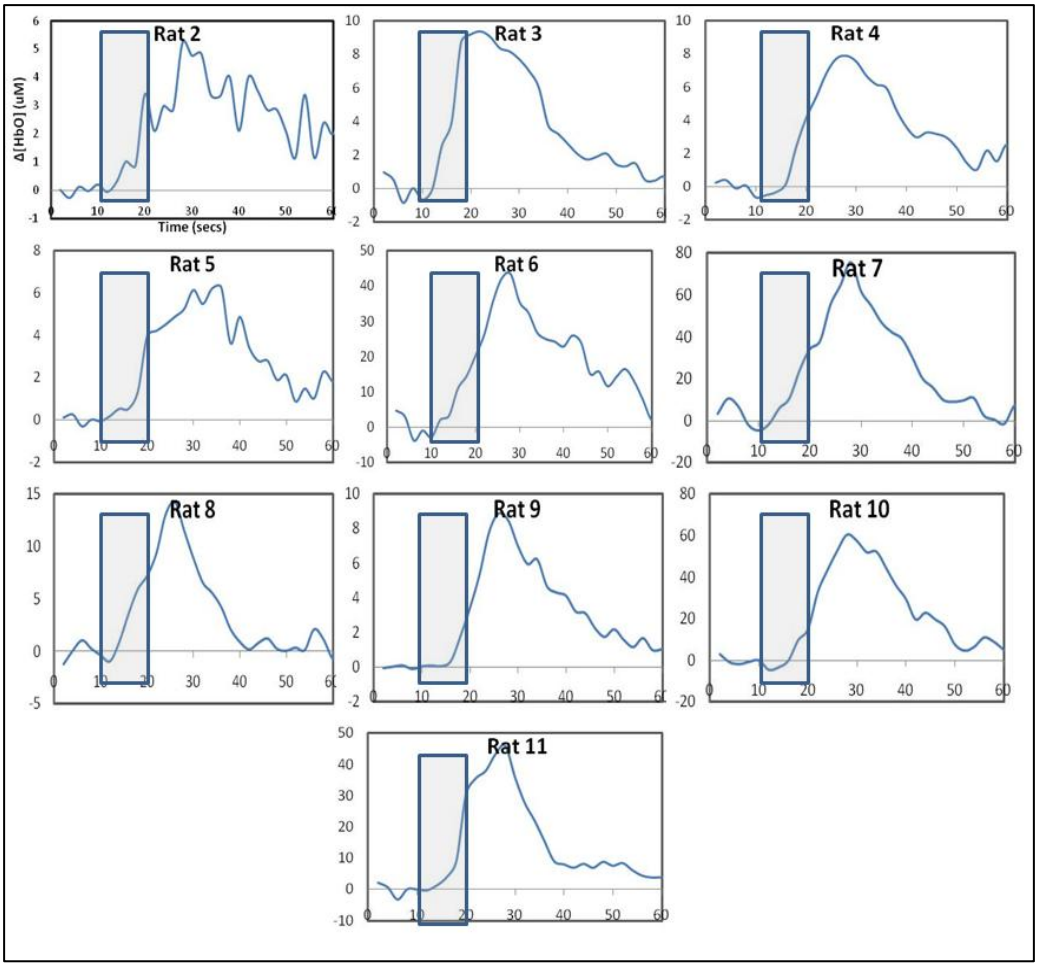

Figure 4.3 An increase in [HbO] at the ipsilateral side of the spinal cord due to electrical stimulation of 10V, 10Hz, 1ms pulse width

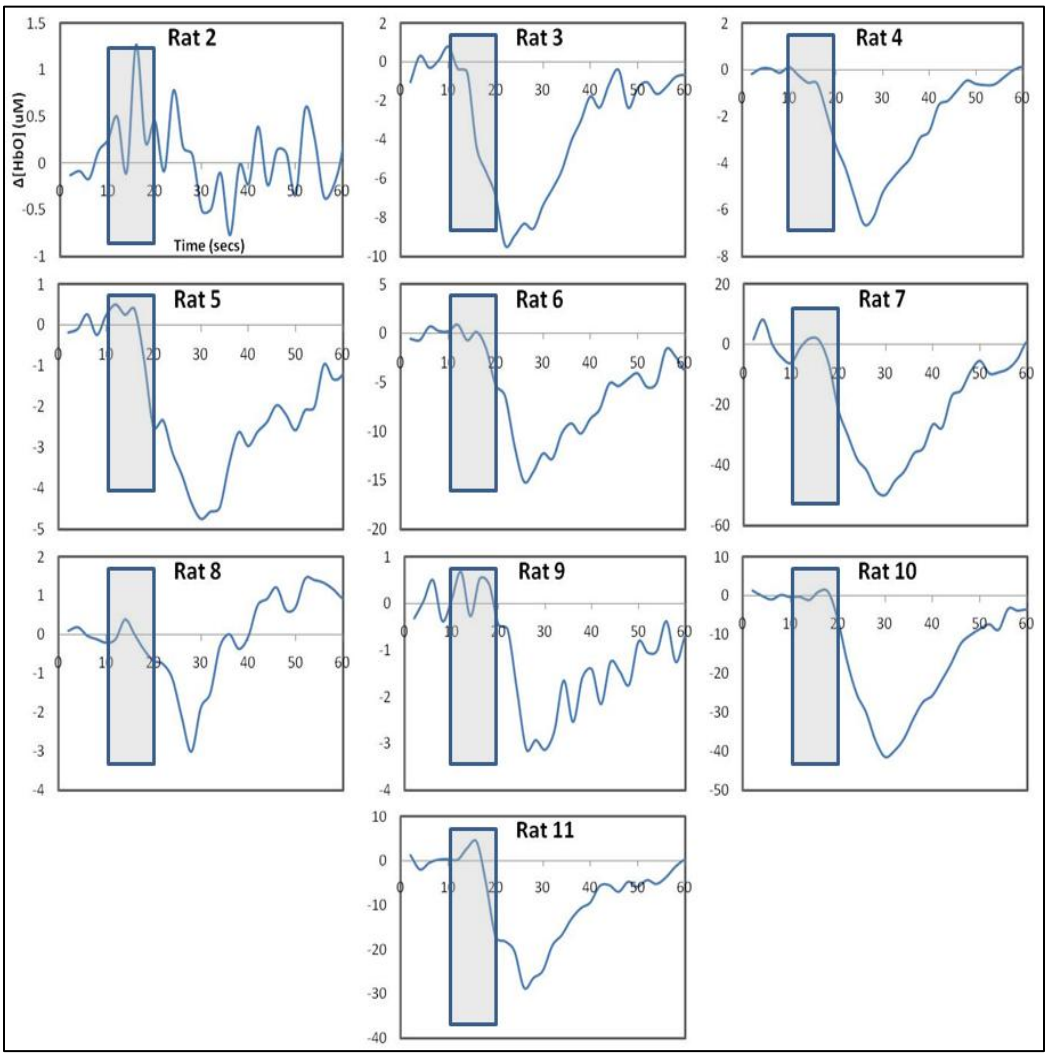

Figure 4.4 A decrease in [Hb] at the ipsilateral side of the spinal cord from the baseline due to electrical stimulation of 5V, 10Hz, 1ms pulse width

Also, all ten-rat data were statistically analyzed for changes in [HbO] and [Hb] at the ipsilateral side of the spinal cord. The results of the statistics are shown in Table 4.2. The p-value is for α of 5%.

Table 4.2 The statistical results for the ipsilateral side of the spinal cord in response to electrical stimulation on the paw.

10V Electrical	P-value (n=10)
[HbO]	0.0008
[Hb]	0.0026

4.4.2 Brain

From past studies, it is seen that mechanical stimulations do not show large changes in [HbO] and [Hb] in somatosensory cortex of the brain [29]. The somatosensory cortex is composed of only a few numbers of nociceptive specific neurons, and these are interspersed with non-nociceptive neurons. Hence, it can be suggested that pure nociceptive stimuli, such as mechanical stimulation, may cause little or no S1 activation in imaging studies [29]. Since the organization of the nociceptive and non-nociceptive neurons is intermixed, the optical probe would pick up signals which are averaged over the entire region of probe location and will not contain information specifically from the nocicpetive neurons in the cortex. This may explain the reason for no changes in [HbO] and [Hb] in the S1 region due to mechanical stimulations, based on the observation through my experiments.

On the other hand, an electrical stimulus indiscriminately activates all local receptors, both nociceptive and non-nociceptive, and therefore results in activation of S1 neurons. This is confirmed by our results, as given in Fig. 4.5.

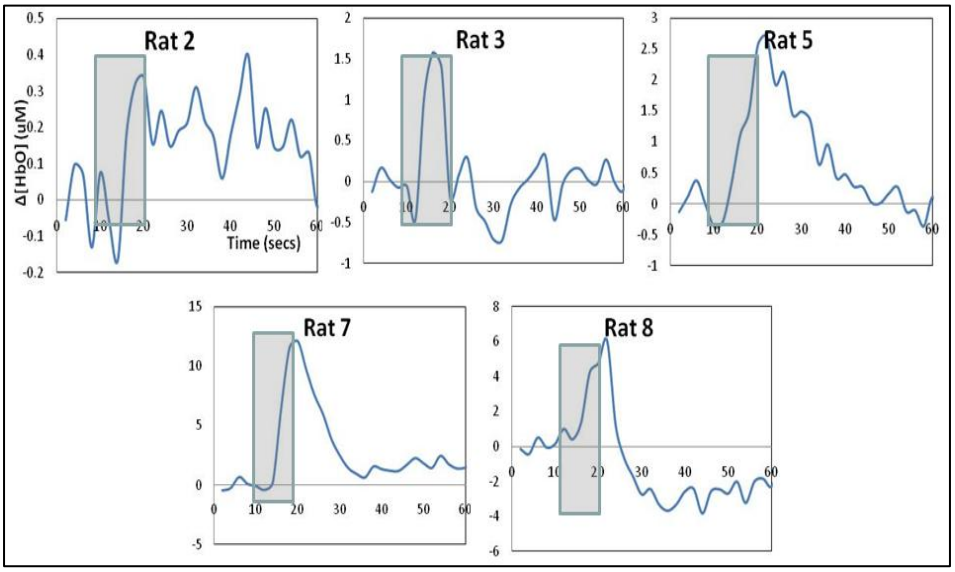

Figure 4.5 The changes in [HbO] at the contralateral side of S1 region in the brain, due to electrical stimulation of 10V, 10Hz and 1ms pulse width.

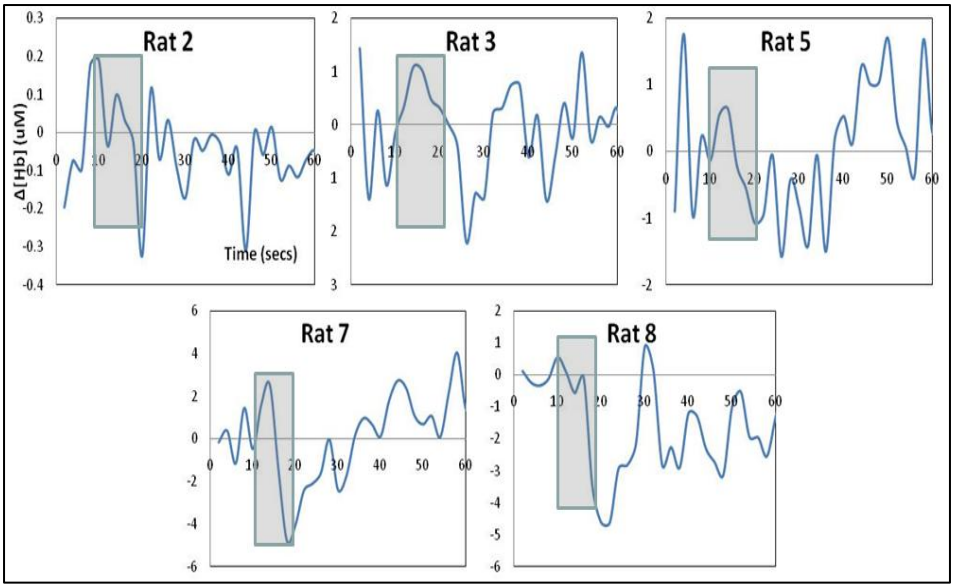

Figure 4.6 A decrease in [Hb] at the contralateral side of the brain in S1 region from the baseline due to electrical stimulation of 10V, 10Hz, 1ms pulse width

The results for the statistical analysis over 5 rats in response to the 10 V, 10 Hz electrical stimulations on S1 region are shown in Table 4.3. The P-value is computed for α of 5%.

Table 4.3 The statistical results on the contralateral side of the brain in response to electrical stimulation (10 V) on the paw.

10V Electrical	P-value (n=5)
[HbO]	0.0356
[Hb]	0.1056

4.4.3 Comparison between Spinal cord and Brain

As seen in my results, the hymodynamic responses to 10-V electrical stimulations are different at the spinal cord from that of the brain. The amplitudes of increase in [HbO] on the spinal cord are much larger as compared to that at the brain. As only five rats showed a change in [HbO], only those rats are compared for their responses on the spinal cord. Table 4.4 shows the maximum amplitude at the spinal cord and the brain, in response to the 10-V electrical stimulation at the paw. As seen from 4.4, there are huge variations of increase in amplitude for [HbO] changes in different rats. This data when plotted on a Q-Q plot, did not show a 45 degree line passing through zero. This means, that the data was not normally distributed. To make it normal distributed data, logarithm of this data set was taken. This is again plotted on Q-Q plots, which showed a 45 degree line passing through zero. Students T-test was then performed on the logarithmic values of the data.

Table 4.4 The maximum amplitude of changes in [HbO] at the spinal cord and the brain, in response to 10-V electrical stimulation at the paw. The p-value < 0.05, shows that they are statistically different.

Subject	Spinal cord	Brain
Rat 2	5.2344	0.39892
Rat 3	9.38328	1.6795
Rat 5	6.25132	2.7073
Rat 7	75.7186	12.4676
Rat 8	14.2142	6.06235
P-value	0.0088	

It is clear from my experimental data that there are differences in hemodynamic responses between the spinal cord and brain. It is reported that in the spinal cord, the neurotransmitter substance P, a vasodilator, is released only by C-fiber but not by A-fiber activation [30]. This contributes to an increase in local blood flow and blood volume. In the brain, the contribution of substance P to vasodilation is minimal [31]. Hence, it is expected that a relatively greater increase in [HbO], as shown in Table 4.4, on the spinal cord may result from the released neurotransmitter substance P by C-fiber.

Furthermore, the rats that were analyzed for 10-V electrical stimulation all had different amplitude of increase in [HbO], in responses on the brain as well as on the spinal cord. For easy comparison, I normalized the individual responses of the rats and averaged them together. Figure 4.7 shows the normalized changes in [HbO], with the standard error of mean plotted, for both the spinal cord and brain, due to 10-V electrical stimulation at the paw. Notice that the brain responses were taken contralaterally and the spinal cord responses were taken ipsilaterally.

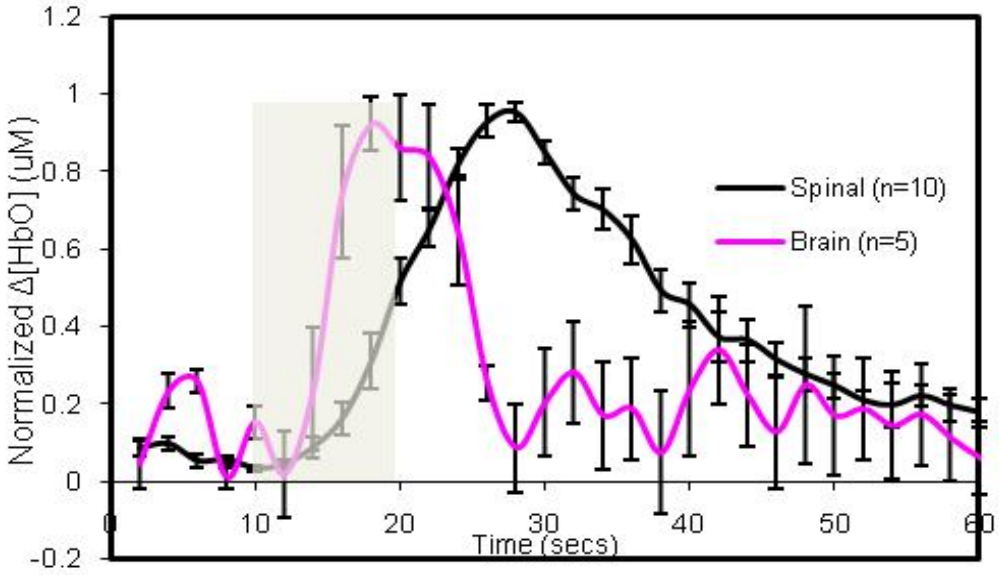

Figure 4.7 The normalized change in [HbO], at the spinal cord and brain, due to 10-V electrical stimulation at the paw

It is interestingly seen that the time-to-peak value is longer (almost double) in the spinal cord response as compared to that in the brain [42]. In principle, the action potentials that fire, due to the pain stimulations, and reach the brain from the spinal cord pathway should be within few milliseconds. A possible explanation for Fig. 4.7 is as follows: under the 10-V electrical stimulation, the neuro-hemodynamic response should be seen in the brain, leading to an increase in [HbO]. The brain then sends motor reflex signals, back through the same pathway, to the paw. Hence, the [HbO] signals on the spinal cord continue to last, due to the reflex signal, lengthening the response time.

To further analyze this difference between the responses times on the spinal cord and the brain due to the same electrical stimulations, I statistically compared the time-to-peak values for both the spinal cord and the brain. Figure 4.8 shows the different time-to-peak values in the two respective cases. It is seen that the [HbO] changes reach its peak earlier at the S1 region of the brain as compared to the spinal cord, almost about one half of the time taken on the spinal cord.

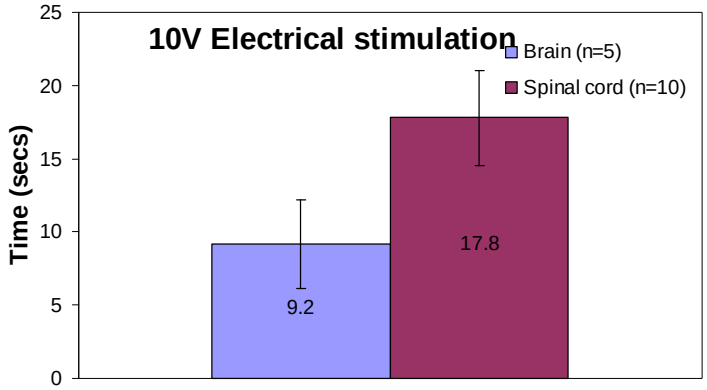

Figure 4.8 The time-to-peak values in [HbO] changes, at the spinal cord and the S1 region in the brain due to 10V electrical stimulation.

Also, to analyze the time spread of the [HbO] changes at the spinal cord and the S1 region of the brain, I calculated the Full width half maxima (FWHM). Figure 4.9 shows the different time spread of the [HbO] changes in these two respective cases due to electrical stimulation of 10V. The time spread on the spinal cord is almost 3 times more than that on the brain.

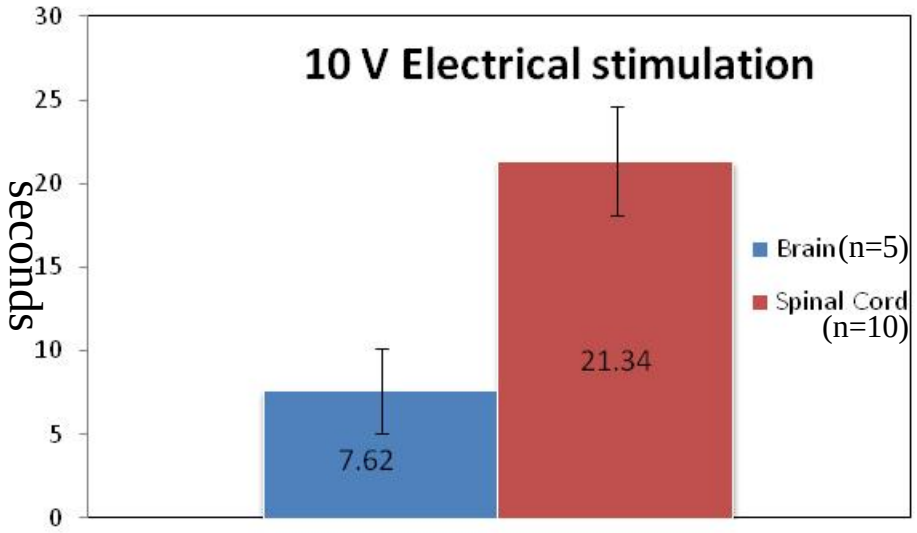

Figure 4.9 The time spread of the [HbO] changes, at the spinal cord and the S1 region in the brain due to 10V electrical stimulation.

4.4.4 Hemodynamic changes using Modified Beer Lambert's Law

Using the reflectance model, it is seen from the previous sections of this chapter, I have obtained the absolute hemodynamic changes. However, the data processing takes time, roughly around 2 minutes per spectrum, due to curve fitting procedures. This would mean more than several hours of data processing for each of the probes used for every rat and impossible for real-time monitoring with this method. Hence, a faster means to achieve relative hemodynamic changes was highly desirable and explored, as mentioned earlier. Namely, the faster approach is based on the modified Beer-Lambert's Law, as explained in details in Chapter 3.

From the phantom experiments, using the modified Beer-Lambert's law, it is seen that changes in [Hb] are influenced by scattering, but [HbO] changes are solely due to changes in the absorption. Knowing this, I have analyzed the [HbO] changes at the spinal cord due to the 10-V electrical stimulations at the paw, to compare the trends with the absolute [HbO] changes. Figure 4.10 shows the relative [HbO] changes from the baseline, at the ipsilateral side of the spinal cord, due to electrical stimulations of 10V at the hind paw. After analyzing the blocks, I block averaged the hemodynamic responses over 5 blocks, as shown in Figure 4.11. Similar trends of changes in [HbO] are clearly seen between Fig. 4.11 and Fig. 4.3. This unambiguously validates the relative method using the modified Beer-Lambert's law and offers a more efficient way for real-time data analysis.

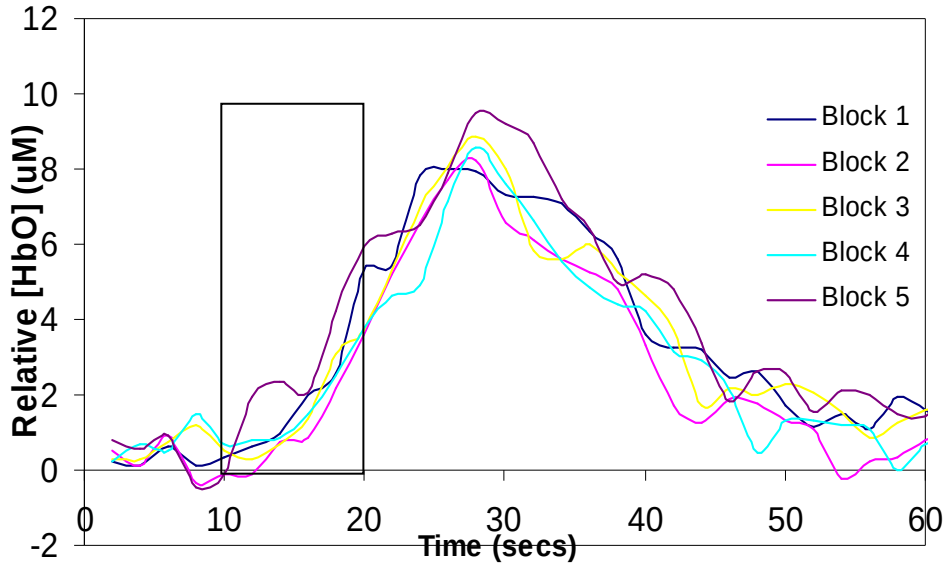

Figure 4.10 The relative [HbO] changes for each of the five blocks, for Rat 7, at the ipsilateral side of the spinal cord, due to electrical stimulation of 10V at the hind paw.

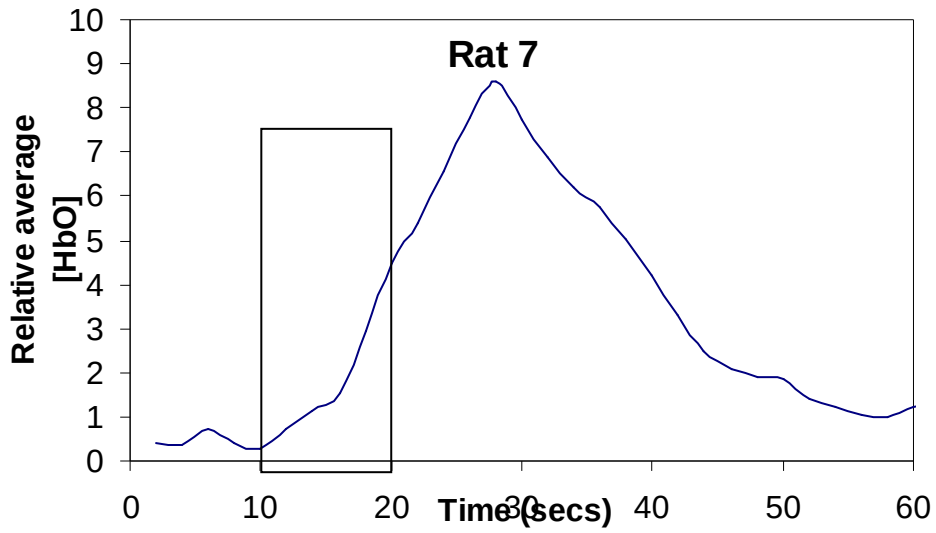

Figure 4.11 The relative average [HbO] changes, for Rat 7, at the ipsilateral side of the spinal cord, due to electrical stimulation of 10V at the hind paw.

CHAPTER 5

CONCLUSION AND FUTURE SCOPE

From the phantom studies, we see that the analytical reflectance model gives us the absolute measures of the hemodynamic changes, while the modified Beer-Lambert's law gives us relative measures in oxy-hemoglobin changes. The reflectance model is a slow processing method, however, as compared to the modified Beer-Lambert's Law. The relative change in [Hb], as determined using the modified Beer-Lambert's law, is greatly influenced by scattering and thus could not be quantified in a faster means, while relative changes in [HbO] are reliable when using modified Beer-Lambert's law.

Both of the methods show a means of successfully calculating hemodynamic changes. To demonstrate these two methods on real measurements and to check the validity on live tissues, I performed pain studies in rats by placing 4 thin fiber probes on the spinal cord and the brain of the animals and recording the optical signals simultaneously during and after electrical stimulations. As seen in the results section of the previous chapter, significant changes in [HbO] during and after electrical stimulations of 10 V given on the animal paw are observed at the ipsilateral side of the spinal cord and the contralateral side of the brain (S1 region).

Only in a few rats, I could see significant hemodynamic changes in the S1 region of the brain due to the electrical stimulation. The reason that I have not completely succeeded in all the brain measurements could be due to the difficulty in placing the probe accurately at S1 region. For future improvement, a better imaging or mapping tool would be surely helpful to guide the optical probe placement at the exact location of S1 somatosensory region.

This study also presents an interesting observation: there exist clear differences in oxy-hemoglobin concentration changes between the responses at the spinal cord and the brain due to the same stimulations. Such differences in [HbO] include amplitude, time-to-peak values, and time spread of the measured hemodynamic signals: the responses in the brain are faster and more prompt with a narrower spread, while the signals on the spinal cord have larger amplitudes with a longer time to reach the peak and a broader spread. The explanation for this observation is very preliminary. Further studies are planned using multiple needle probes on the S1 region of the brain and on various locations at the spinal cord with a large sample size to confirm my finding and understand possible underlying mechanism.

My study demonstrates the usefulness and feasibility to use an optical reflectance spectroscopy and multiple thin fiber-optic probes for investigating hemodynamic responses to pain stimulations, such as mechanical, electrical, and chemical stimulations, at multiple sites along the central nervous system. Overall, through this study, I conclude that this simple optical method can be utilized as a real-time monitoring tool to characterize and quantify temporal changes in blood circulation and concentration during peripheral pain stimulations; it can be also useful in understanding different pain mechanisms and quantifying peripheral blood volume changes in response to pain.

APPENDIX A

PHOSPHATE BUFFERED SALINE

Phosphate Buffered Saline (PBS)

10X PBS (0.1M PBS, pH 7.2):

Na2HPO4 (anhydrous) ---------- 10.9 g

NaH2PO4 (anhydrous) ---------- 3.2 g

NaCl ---------- 90 g

Distilled water ---------- 1000 ml

Mix to dissolve and adjust pH to 7.2

Store this solution at room temperature. Dilute 1:10 with distilled water before use and adjust pH if necessary

REFERENCES

[1] B. Chance, S. Nioka, J. Kent, K. McCully, M. Fountain, R. Greenfeld, and G. Holtom, "Time-resolved spectroscopy of hemoglobin and myoglobin in resting and ischemic muscle," Analytical Biochemistry, vol. 174, pp. 698-707, (1988).

[2] S. Homma, T. Fukunaga, and A. Kagaya, "Influence of adipose tissue thickness on near infrared spectroscopic signal in the measurement of human muscle," Journal of Biomedical Optics, vol. 1, pp. 418-424, (1996).

[3] M. Ferrari, Q. Wei, L. Carraresi, R. A. De Blasi, and G. Zaccanti, "Time-resolved spectroscopy of the human forearm," Journal of Photochemistry and Photobiology B: Biology, vol. 16, pp. 141-153, (1992).

[4] B. Chance, E. Anday, S. Nioka, S. Zhou, L. Hong, K. Worden, C. Li, T. Murray, Y. Ovetsky, D. Pidikiti, and R. Thomas, "A novel method for fast imaging of brain function, non-invasively, with light," Optics Express, vol. 2, pp. 411-423, (1998).

[5] R. Wenzel, H. Obrig, J. Ruben, K. Villringer, A. Thiel, J. Bernarding, U. Dirnagl, and A. Villringer, "Cerebral blood oxygenation changes induced by visual stimulation in humans," Journal of Biomedical Optics, vol. 1, pp. 399-404, (1996).

[6] D. Kashyap, V. Sharma, and H. Liu, "Non-invasive monitoring of hemodynamic changes in orthotropic brain tumor," presented at Optical Tomography and Spectroscopy of Tissue VII, San Jose, CA, USA, (2007).

[7] H. Liu, Y. Song, K. L. Worden, X. Jiang, A. Constantinescu, and R. P. Mason, "Noninvasive investigation of blood oxygenation dynamics of tumors by near-infrared spectroscopy," Applied Optics, vol. 39, pp. 5231-5243, (2000).

[8] M. Johns, C. Giller, and H. Liu, "Computational and in vivo investigation of optical reflectance from human brain to assist neurosurgery," Journal of Biomedical Optics, vol. 3, pp. 437-445, (1998).

[9] M. Johns, C. A. Giller, and H. Liu, "Determination of hemoglobin oxygen saturation from turbid media using reflectance spectroscopy with small source-detector separations," Applied Spectroscopy, vol. 55, pp. 1686-1694, (2001).

[10] C. A. Giller, H. Liu, P. Gurnani, S. Victor, U. Yazdani, and D. C. German, "Validation of a near-infrared probe for detection of thin intracranial white matter structures," Journal of Neurosurgery, vol. 98, pp. 1299-1306, (2003).

[11] H. Liu, Y. Gu, J. G. Kim, and R. P. Mason, "Near-Infrared Spectroscopy and Imaging of Tumor Vascular Oxygenation," Methods in Enzymology, vol. 386, pp. 349-378, (2004).

[12] G. Zonios and A. Dimou, "Modeling diffuse reflectance from semi-infinite turbid media: application to the study of skin optical properties," Optics Express, vol. 14, pp. 8661-8674, (2006).

[13] T. J. Farrell, M. S. Patterson, and B. Wilson, "A diffusion theory model of spatially resolved, steady-state diffuse reflectance for the noninvasive determination of tissue optical properties in vivo," Medical Physics, vol. 19, pp. 879-888, (1992).

[14] E. L. Hull and T. H. Foster, "Steady-state reflectance spectroscopy in the P_3 approximation," Journal of the Optical Society of America A, vol. 18, pp. 584-599, (2001).

[15] M. Johns, C. A. Giller, D. German, and H. Liu, "Determination of reduced scattering coefficient of biological tissue from a needle-like probe," Optics Express, vol. 13, pp. 4828-4842, (2005).

[16] S. J. Matcher, M. Cope, and D. T. Delpy, "In vivo measurements of the wavelength dependence of tissue-scattering coefficients between 760 and 900 nm measured with time-resolved spectroscopy," Applied Optics, vol. 36, pp. 386-396, (1997).

[17] S. T. Flock, S. L. Jacques, B. C. Wilson, W. M. Star, and M. J. C. Van Gemert, "Optical properties of intralipid: A phantom medium for light propagation studies," Lasers in Surgery and Medicine, vol. 12, pp. 510-519, (1992).

[18] http://www.oceanoptics.com/Products/ws1diffrefstan.asp, "Diffuse Reflectance Standards," Ocean Optics Inc, (2007).

[19] E. R. Kandel, J. H. Schwartz, and T. M. Jessell, Principles of Neural Science, 4 ed: McGraw-Hill Professional, (2000).

[20] R. Benesch, G. Macduff, and R. E. Benesch, “Determination of oxygen equilibria with a versatile new tonometer,” *Anal. Biochem.*, 11, 81-87 (1965).

[21] O. W. van Assendelft and W. G. Zijlstra, “Extinction coefficients for use in equations for the spectrophotometric analysis of hemoglobin mixtures,” *Anal. Biochem.*, 69, 43-48 (1975).

[22] R. E. Benesch, R. Benesch, and S. Yung, “Equations for the spectrophotometric analysis of hemoglobin mixtures,” *Anal. Biochem.*, 55, 245-248 (1973).

[23] W. G. Zijlstra, A. Buursma, and W. P. Meeuwsen-van der Roest, "Absorption spectra of human fetal and adult oxyhemoglobin, deoxyhemoglobin, carboxyhemoglobin, and methemoglobin," *Clin. Chem*. 37, 1633–1638 (1991).

[24] "Responses of a spino-olivo-cerebellar pathway in the cat" by d. M. Armstrong* and r. J. Harvey

[25] "Look-Ahead Distance" of a probe used to assist neurosurgery: Phantom and Monte Carlo Study. Zhiyu Qian, Sunder S. Victor, Yueqing Gu, Cole A. Giller, Hanli Liu. (2003)

[26] "Prolonged noxious mechanical stimulation of the rat's tail: responses and encoding properties of dorsal horn neurones." F Cervero, H O Handwerker and J M Laird

[27] "Ascending Projections of Nociceptor-driven Lamina I Neurones in the Cat" F. Cervero, A. Iggo, and V. Molony

[28] "BOLD and blood volume-weighted fMRI of rat lumbar spinal cord during non-noxious and noxious electrical hindpaw stimulation" Fuqiang Zhao,a, Mangay Williams, Xiangjun Meng, Denise C. Welsh, Alexandre Coimbra, Eric D. Crown, Jacquelynn J. Cook, Mark O. Urban, Richard Hargreaves, and Donald S. Williamsa (2007).

[29] "Comparative effect of thermal, mechanical, and electrical noxious stimuli **on** the electroencephalogram of the rat" J. C. Murrell*****, S. L. Mitchinson, D. Waters and C. B. Johnson. (2007)

[30] Schaible, H.G., Jarrott, B., Hope, P.J., Duggan, A.W., 1990. "Release of immunoreactive substance P in the spinal cord during development of acute arthritis in the knee joint of the cat: a study with antibody microprobes."

[31] Freedman, J., Post, C., Kahrstrom, J., Ohlen, A., Mollenholt, P., Owman, C., Alari, L., Hokfelt, T., 1988. "Vasoconstrictor effects in spinal cord of the substance P antagonist [D-ARG1, D-ARP7,9, LEU11]—substance P (spantide) and somatostain and interaction with thyrotropin releasing hormone."

[32] www.nirx.net

[33] "Development of a Broadband Multi-Channel NIRS System for Quantifying Absolute Concentrations of Hemoglobin Derivatives and reduced scattering Coefficients" Dissertation By Dheerendra Kashyap

[34] "Pain Perception" By Gary Reiness (2005).

[35] "Animal Models of Nociception" Daniel Le Bars, Manuela Gozariu, and Samuel W. Cadden(2001).

[36] “Model Driven Analysis of Optical Reflectance Spectroscopy for Detection Of Human Prostate and Kidney Cancers” Thesis by Aditya Mathker

[37] W. G. Zijlstra, V. O. W. Assendelft, and A. Buursma, Visible and Near Infrared “Absorption Spectra of Human and Animal Haemoglobin: Determination and Application: VSP, (2000).”

[38] www.stahlonline.cambridge.org

[39] www.continuingedcourses.net

[40] www.illuminationtech.com

[41] www.oceanoptics.com

[42] “A hemodynamic response function for functional MRI of the cervical spine using motor and nociceptive paradigms” J. E. Brown1, D. S. Watcha, J. Darnauer, R. Sarin4, G. Glover, and S. Mackey (2007).

[43] “Investigation of Breast Tumor Hemodynamics by Near Infrared Spectroscopy: Applications to Cancer Therapy Monitoring” Dissertation by Jae Gwan Kim

BIOGRAPHICAL INFORMATION

Sweta Narvenkar was born on April 19, 1985, in Goa, India. She received her Bachelor of Engineering degree in Biomedical Engineering from D. J Sanghvi, Mumbai University, Mumbai, India in June 2007. In Fall 2007 she started her graduate studies in Biomedical Engineering from Joint Program of Biomedical Engineering at the University of Texas at Arlington and University of Texas Southwestern Medical Center at Dallas, completing it by Fall 2009. Her research interests include Near Infrared Spectroscopy and medical imaging techniques.